

Quantum precursors to Kolmogorov-Arnold-Moser theorem in Floquet spin- J systems

Jesús A. Segura-Landa^{1,2}, Meenu Kumari^{3,4}, Daniel J. Nader⁵,

Sercan Hüsnügil^{4,6}, Ali SaraerToosi^{4,7}, and Sergio Lerma-Hernández^{1†}

¹Facultad de Física, Universidad Veracruzana, Campus Arco Sur, Paseo 112, C.P. 91097 Xalapa, Mexico.

²Instituto de Ciencias Nucleares, Universidad Nacional Autónoma de México,

Apdo. Postal 70-543, C.P. 04510 Cd. Mx., Mexico

³Digital Technologies, National Research Council Canada

⁴Perimeter Institute for Theoretical Physics, Waterloo ON N2L 2Y5, Canada

⁵Department of Optics, Faculty of Science, Palacky University, Olomouc, 77900, Czech Republic

⁶Department of Physics and Astronomy, University of Waterloo, Waterloo, Ontario, N2L 3G1, Canada and

⁷Department of Computer Science, University of Toronto,

40 St. George St., Toronto, ON, M5S 2E4, Canada

The Kolmogorov-Arnold-Moser (KAM) theorem proves that the resonant tori of classical integrable Hamiltonians are broken when a non-integrable perturbation is introduced, whereas non-resonant tori only get deformed for up to a finite value of the perturbative parameter. In this letter, we identify quantum precursors to the KAM theorem in one-degree-of-freedom spin Hamiltonians periodically perturbed by instantaneous kicks. After recognizing quantum signatures of resonances in the Floquet eigenstates of the perturbed Hamiltonian, we reveal a differentiated sensitivity to the perturbation of the eigenstates of the unperturbed Hamiltonian, depending on whether the states satisfy a resonant condition or not. It is also shown that this differentiated sensitivity becomes more pronounced as the system size increases, leading to the KAM theorem in the classical limit $J \rightarrow \infty$. Numerical and analytical results obtained from unitary perturbation theory strongly support these findings. Although specific to kicked models, our results can be easily extended to more general scenarios, allowing the identification of the quantum mechanism that corresponds to the KAM theorem in the classical limit.

Introduction.— A system is Liouville integrable in classical physics if it has as many independent conserved quantities as degrees of freedom, and their Poisson brackets vanish pairwise [1]. The Kolmogorov-Arnold-Moser (KAM) theorem forms a cornerstone in classical physics demonstrating that weakly perturbed integrable systems retain most properties of integrability for sufficiently small perturbations [1–4]. In quantum physics, while the extremes of fully integrable and globally chaotic systems are relatively well understood, the integrability-to-chaos transition and the dynamics of weakly perturbed integrable systems remain elusive. The search for a quantum analog of the KAM theorem has been ongoing for decades [5, 6]. Recent studies have explored weakly perturbed integrable quantum systems from various perspectives, including the effects of perturbation on the conserved quantities [6–9], eigenvalues and spectral statistics [10], and eigenstates [8, 11]. Additionally, dynamical probes such as out-of-time-order correlators (OTOCs) [10] and quench dynamics [12] have also been studied in such systems, among other quantities of interest [13–16]. These studies have revealed phenomena such as prethermalization plateaus, where local observables relax to nonthermal values at intermediate times [12], scaling properties of perturbation strengths as a function of system size when the system transitions to chaos [17], and the persistence of quasiconserved charges up to specific time scales

[8]. These findings underscore the intricate nature of the integrability-chaos transition [18], offering insights into how classical KAM-like stability might manifest in quantum systems.

In this letter, we address two key questions: (a) What are the manifestations of classical KAM theorem, specifically of classical resonant and non-resonant tori, in the quantum realm, (b) Can the classical KAM theorem be qualitatively recovered from quantum physics? We explore these questions in integrable quantum systems with a semiclassical limit characterized by a single degree of freedom, subject to weak perturbations in the form of periodic kicks. Specifically, we study time-dependent spin- J Hamiltonians of the following form:

$$\hat{H}(t) = \hat{H}_0(\vec{J}) + \epsilon \hat{K}(\vec{J}) \sum_{n=-\infty}^{\infty} \delta(t - n\tau), \quad (1)$$

where $\vec{J} = (\hat{J}_x, \hat{J}_y, \hat{J}_z)$ with $[\hat{J}_i, \hat{J}_j] = i\epsilon_{ijk}\hat{J}_k$ ($\hbar = 1$), and $\hat{H}_0(\vec{J})$ and $\hat{K}(\vec{J})$ describe quantum systems with well-defined semiclassical limits ($1/\hbar_{\text{eff}} \equiv J \rightarrow \infty$) with one-degree-of-freedom. Such systems have been widely studied in contexts including quantum integrability and chaos [19–28], entanglement [29–34], quantum simulation and trotterization [35–37], time crystals [38, 39], and have also been experimentally realized [40–42]. Classically, the periodic kicks with time period τ introduce non-integrability, modulated by the dimensionless perturbation strength ϵ [19]. For small ϵ , the system remains quasi-integrable, preserving non-resonant tori with deformations as predicted by the classical KAM theorem. On the other hand, resonant tori are destroyed,

* mkumari@uwaterloo.ca

† slerma@uv.mx

leading to the emergence of elliptic and hyperbolic fixed points according to the Poincaré-Birkhoff theorem. In the quantum counterpart, manifestations of such behavior are expected to occur [43–45], particularly on the phase-space representation of the quantized stationary states of the complete Hamiltonian. Using floquet theory [46, 47], we classify the quantum system’s eigenstates into resonant and non-resonant via numerical and analytical calculations using unitary perturbation theory [36, 48]. The stroboscopic stationary states are identified as eigenvectors, $|f_k\rangle$, of the Floquet operator, $\hat{F}|f_k\rangle = \exp(-i\phi_k)|f_k\rangle$, with quasi-energies ϕ_k and

$$\hat{F} = \hat{F}_0 \hat{F}_k = \exp\left(-i\tau\hat{H}_0\right) \exp\left(-ie\hat{K}\right). \quad (2)$$

Our findings reveal distinct sensitivity of eigenstates of \hat{H}_0 to perturbations, characterized by the strength of the periodic kicks ϵ relative to the system size J . In the classical limit $J \rightarrow \infty$, we find that resonant eigenstates break down at $\epsilon = 0$, while non-resonant states persist up to $\epsilon \propto \mathcal{O}(1)$, effectively recovering the classical KAM theorem for spin- J systems. Such a classification of Floquet eigenstates is consistent with recent studies on quantum many-body resonances [17, 49–52], and we uniquely quantify their sensitivity relative to system size, identifying quantum precursors to the KAM theorem.

Quantum resonances and their manifestations.— Classically, in a one-degree-of-freedom periodically kicked system with period τ and non-linear Hamilton equations of motion, an $m:n$ resonance takes place when the resonant condition is fulfilled

$$nT(E) = m\tau, \quad n, m \in \mathbb{Z}, \quad (3)$$

where $T(E)$ is the classical time period of the orbit of H_0 with energy E . Such an $m:n$ resonance is associated with an m -cycle in the phase space. In quantum mechanics, it is also possible to establish a resonant condition. For this goal, we first define the quantum periods $T_{k,m}$ as ($m > 0$)

$$T_{k,m} = \frac{2\pi}{E_{k+m} - E_k} \xrightarrow{J \rightarrow \infty} \frac{2\pi}{m(E_{k+1} - E_k)} = \frac{T_{k,1}}{m}, \quad (4)$$

where E_k are the ordered quantized energy levels of Hamiltonian \hat{H}_0 , i.e. $\hat{H}_0|E_k\rangle = E_k|E_k\rangle$ with $E_{k+1} > E_k$. This quantum period is the inverse of the transition frequency between states with indices k and $k + m$. For $m = 1$ (nearest neighbors), the equation above reduces to the semiclassical approximation of the classical periods [54] $T_{k,1} \approx T(\bar{E})$ with $\bar{E} = (E_{k+1} + E_k)/2$. Moreover, from Eq. (4), it follows that the quantum resonant condition is

$$nT_{k,m} = \tau \quad \text{or} \quad \tau(E_{k+m} - E_k) = 2\pi n. \quad (5)$$

The integer number m enters into the previous quantum resonant condition by involving m -th neighbor states [see inset in Fig.1(b)]. Eq.(5) reduces to the classical resonant condition (3) in the classical limit $J \equiv 1/\hbar_{\text{eff}} \rightarrow \infty$.

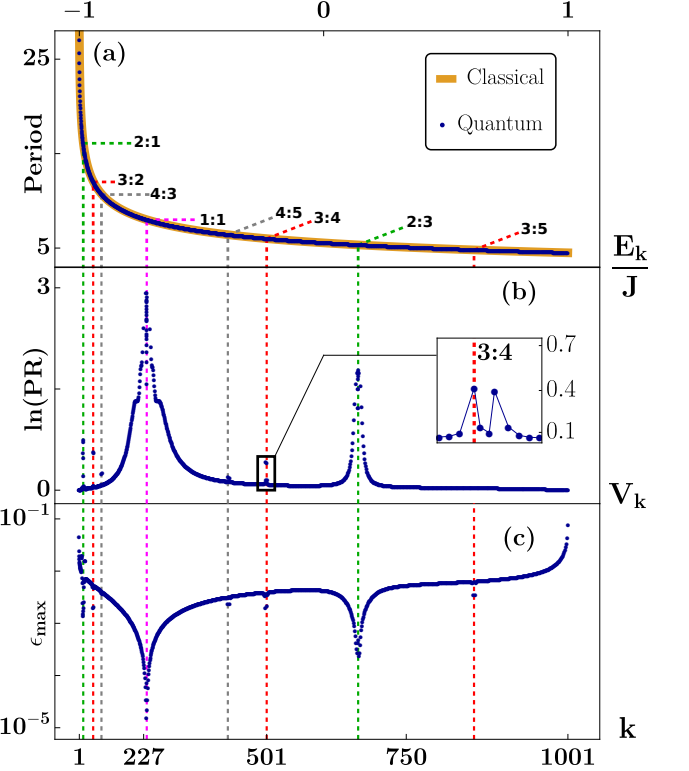


FIG. 1. (a) Classical time period (orange curve) and quantum periods, $T_{k,1} = 2\pi/(E_{k+1} - E_k)$ (black dots), as a function of energy of h_0 (classical) and scaled energies, $\bar{E}_k/J = (E_{k+1} + E_k)/(2J)$ (quantum). (b) Logarithm of the participation ratio of the Floquet eigenstates, $|f_k\rangle$ ’s plotted as a function of $V_k = \langle f_k | \hat{H}_o | f_k \rangle / J$. The inset is a zoom of the 3:4 resonance, showing that third neighbours states are involved in this resonance. (c) Maximum perturbation strength $\epsilon_{k,\max}$, Eq.(7), as a function of the index k of the Floquet eigenstates $|f_k\rangle$ associated, respectively, to the states $|E_k\rangle$. Dashed lines with labels $m:n$ in the panels indicate some rational multiples of the kick period $m\tau/n$ and the energies associated, $E_{m:n}$. Parameters used: $J = 500$ and $\tau = 8$ for (a-c), and $\epsilon = 10^{-3}$ for (b). Data for (c) available at [53]

In order to illustrate the quantum and classical manifestations of the resonances in an experimentally realizable scenario, we consider as the time-independent term, the Hamiltonian of the Lipkin-Meshkov-Glick (LMG) model [55] in the pseudo spin representation [56–59]

$$\hat{H}_0 = \hat{J}_z + \frac{\gamma_x}{2J-1} \hat{J}_x^2 + \frac{\gamma_y}{2J-1} \hat{J}_y^2, \quad (6)$$

with control parameters $\gamma_x = -0.95$ and $\gamma_y = 0$, and the kicking term in (1) as $\hat{K} = \hat{J}_z + \hat{J}_x$. This selection is beneficial for the manifestations of the resonances for two reasons: i) the density of states, $\rho(\bar{E}) = T_{k,1}/(2\pi)$, of the LMG model for this parameter is free of singularities—the so-called Excited State Quantum Phase Transitions (ESQPTs) [60]— and ii) the chosen kick operator has matrix elements $\langle E_{k+m} | \hat{K} | E_k \rangle \neq 0$ whose modulus de-

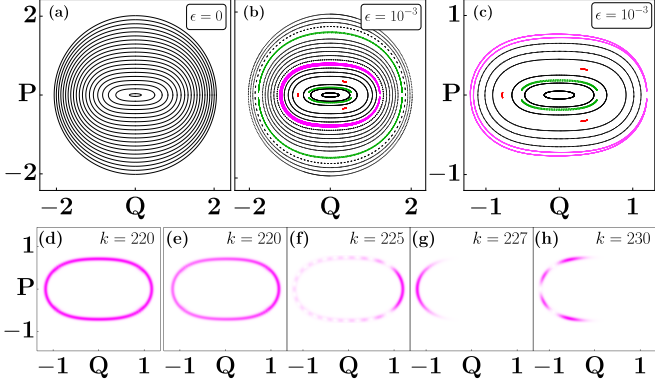


FIG. 2. *First row:* stroboscopic Poincaré sections of the classical LMG Hamiltonian (a) without and (b) with a small perturbation; (c) a zoom of the low-energy region of (b). *Second row:* (d) Husimi function of a representative LMG eigenstate in that energy region, and (e)-(h) of Floquet eigenstates close to 1:1 resonance. Parameters used: $\tau = 8$ and $\epsilon = 10^{-3}$, and for second row $J = 500$.

creases with m , which turns out to be essential towards a clearer manifestation of the resonances as we will show below. After considering possible particularities in the \hat{H}_0 spectrum, such as degeneracies or avoided crossings, more general scenarios can be analyzed similarly. The terms in $\hat{H}(t)$ scale linearly with J , therefore the classical limit can be easily obtained by considering $h(Q, P) = h_0 + \epsilon k \sum \delta(t - n\tau) \equiv \lim_{J \rightarrow \infty} \langle \alpha | \hat{H}(t) | \alpha \rangle / J$, with Bloch coherent states $|\alpha\rangle = [e^{\alpha \hat{J}^+} / (1 + |\alpha|^2)^J] |J, -J\rangle$, where the complex parameter of the Bloch coherent states is expressed as $\alpha(Q, P) = (Q - iP) / \sqrt{4 - (Q^2 + P^2)}$ [61, 62].

In Fig.1(a), we show the time period T of the classical LMG Hamiltonian h_0 [63] along with the quantum periods $T_{k,1} = 2\pi/(E_{k+1} - E_k)$ plotted versus the respective mean energy $\bar{E}_k/J = (E_{k+1} + E_k)/(2J)$. Quantum and classical periods are barely distinguishable. In the same figure, horizontal and diagonal dashed lines indicate some rational multiples of the kick period $m\tau/n$ with $\tau = 8$; resonances appear for trajectories of h_0 with energy $E_{m:n}/J$ (corresponding vertical dashed lines). Consequently, the corresponding tori are destroyed as it is illustrated in the stroboscopic Poincaré sections shown in panels (a)-(c) of Fig. 2, where resonant trajectories are highlighted in magenta for resonance 1:1; in green for resonances 2:1 and 2:3; and in red for resonance 3:2.

Quantum resonances can be revealed by studying the localization of the Floquet eigenstates on the \hat{H}_0 energy basis $|E_k\rangle$ through the Participation Ratio [64, 65], defined as $\text{PR}_k = 1/\sum_n |\langle E_n | f_k \rangle|^4$. This quantity is plotted as a function of the expectation value $V_k = \langle f_k | \hat{H}_0 | f_k \rangle / J$, in Fig. 1(b). The resonances manifest as a sudden increase in PR_k , which reflects that, close to a resonant condition, Floquet eigenstates spread across the \hat{H}_0 eigenbasis. Quantum resonances manifest even if, due to the discreteness of the values of $T_{k,m}$, the quantum resonant condition may not be

exactly fulfilled. Meanwhile, in the classical picture, the continuity of T guarantees that the resonant conditions are always exactly satisfied. When the quantum resonant condition is exactly satisfied, the resonant effects are more prominent [63]. Quantum manifestations of the resonances can also be observed in the phase space quasi-probability distribution functions of the Floquet eigenstates, such as Husimi functions. The Husimi function, $\mathcal{Q}_k(P, Q) = |\langle \alpha(Q, P) | f_k \rangle|^2$, of Floquet eigenstates close to the 1:1 resonance are shown in Figs. 2(e)-(h). Eigenstate with index $k = 220$ is far enough from the resonant condition, such that its Husimi function is very similar to those of the LMG eigenstates, $\tilde{\mathcal{Q}}_n(P, Q) = |\langle \alpha(Q, P) | E_n \rangle|^2$, as the one in Fig. 2(d). In contrast, states closer to the resonance ($k = 225, 227$, and 230) concentrate within the region of the classical broken tori, exhibiting a pattern of nodes and antinodes, as previously reported in Refs. [43–45, 66] for other models.

Classically, according to the KAM theorem, a resonant condition breaks the h_0 tori even for an infinitesimal perturbation ϵ . In contrast, in the quantum case, the Floquet eigenstates for infinitesimal ϵ can be unequivocally identified with energy eigenstates of the unperturbed Hamiltonian \hat{H}_0 . As ϵ increases, this unequivocal identification for $|f_k\rangle$ continues if its maximum overlap with the eigenstates of \hat{H}_0 satisfies [67] $\mathcal{F}_{k,\max} \equiv \max_n |\langle f_k | E_n \rangle|^2 > \frac{1}{2}$. The equality

$$\mathcal{F}_{k,\max} = 1/2 \quad (7)$$

defines the maximum value of ϵ for which the Floquet eigenstate $|f_k\rangle$ can be associated unequivocally with a single eigenstate of \hat{H}_0 . We denote this perturbation value as $\epsilon_{k,\max}$, and it is the quantum equivalent of the perturbation strength at which KAM tori break in the classical case. The resilience of the \hat{H}_0 eigenstates to the perturbation is gauged by $\epsilon_{k,\max}$ and it is significantly smaller for states close to a quantum resonant condition. This is illustrated in Fig. 1(c), where $\epsilon_{k,\max}$ is plotted for all the Floquet eigenstates against the energy of the corresponding \hat{H}_0 eigenstate with which they are associated. From this figure, it is clear that $\epsilon_{k,\max}$ is highly sensitive to the quantum resonant condition, exhibiting a sudden decrease close to the resonances. These dips become more prominent as we increase J and approach the classical limit. In the following, by studying the behavior of $\epsilon_{k,\max}$ in the classical limit $J \equiv 1/\hbar_{\text{eff}} \rightarrow \infty$, we not only recover the KAM theorem but also identify its quantum precursors for large but finite J .

Scaling of ϵ_{\max} .— We study the scaling properties of ϵ_{\max} with J under three different conditions: non-resonant NR, close to resonant CR, and exact resonant ER, with a clear distinct scaling behavior of ϵ_{\max} . For the latter two, we select the most notable resonances of Fig.1, namely 1:1, and 2:3. As discussed in [63], a similar analysis for other resonances would require numerical

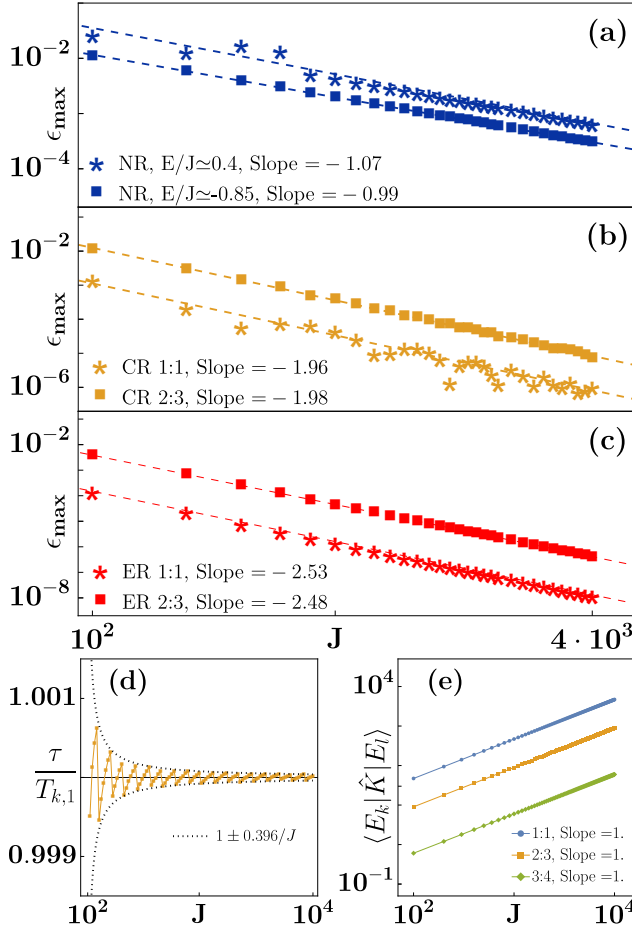


FIG. 3. (a) ϵ_{\max} as a function of J in log-log scale for non-resonant states, (b) states close to resonance and (c) exact resonant states. Numerical fits to the numerical data are indicated in each panel. (d) Time period of the kick over its closest quantum period, $\tau/T_{k,1}$, as a function of J in linear-linear scale. The exact resonant condition 1:1 is $\tau/T_{k,1} = 1$ (see [63] for similar plots for other resonances). (e) Scaling of kick matrix elements for states involved in resonances 1:1 ($l = k + 1$), 2:3 ($l = k + 2$) and 3:4 ($l = k + 3$). In panels (a), (b) and (d) the kick period is $\tau = 8$. In panel (c) τ is adjusted to fulfill exactly the quantum resonant conditions with $\tau \approx 8$. Non-resonant states in (a) are obtained by selecting \hat{H}_0 eigenstates closest to the energies $E/J = 0.4$ and $E/J = -0.85$, where, according to Fig.1, no resonances are present. Data for (a-c) available at [53].

simulations with much larger J values, which are significantly more computationally expensive.

The non-resonant condition is obtained by fixing τ (we use $\tau = 8$) and, for each J , selecting the state in the \hat{H}_0 spectrum that closely satisfies $\tau/T_{k,1} = f$, where f is a floating point approximation of an irrational number, in our case we select $f = 8/T(\varepsilon)$, where $T(\varepsilon)$ is the classical time period of h_o at the classical energy $\varepsilon \equiv E/J = -0.85$ and 0.4 . The condition close to the resonance $m:n$ is obtained by fixing τ and, for

each J , selecting the state $|E_k\rangle$ in the \hat{H}_0 spectrum that comes closest to satisfying the resonant condition $\frac{\tau}{nT_{k,m}} = \frac{\tau(E_{k+m} - E_k)}{2\pi n} = 1$. Due to the discreteness of the spectrum, the resonant condition is not exactly satisfied, but it becomes closer to being fulfilled as J increases. This is illustrated in Fig. 3(d), where it is observed that the ratio $\frac{\tau}{nT_{k,m}}$ oscillates around 1 with an amplitude that decreases proportionally to $1/J$. Finally, for the exact resonant condition, a two-step process is employed. First, we follow a similar approach as in the close to resonance condition. Then, for each value of J , we fine-tune the kicking period τ to exactly satisfy the condition $\frac{\tau(E_{k+m} - E_k)}{2\pi n} = 1$.

In panels (a)-(c) of Fig. 3, we show the scaling of ϵ_{\max} for these three distinct conditions: (a) non-resonant, (b) close to resonance and (c) exact resonant. In all cases, ϵ_{\max} goes to zero following a power law, but at different rates. For resonant states ϵ_{\max} approaches zero faster than for non-resonant states. For non-resonant states, we obtain $\epsilon_{\max}^{\text{NR}} \approx AJ^{-1}$, whereas for close to resonance and exact resonant states we obtain, respectively, $\epsilon_{\max}^{\text{CR}} \approx BJ^{-2}$ and $\epsilon_{\max}^{\text{ER}} \approx CJ^{-5/2}$. These differentiated scalings constitute a significant finding of this letter, they are quantum precursors of the classical KAM theorem, and lead to the KAM theorem in the classical limit as follows: for pseudospin models, the classical Hamiltonian is obtained from $h_{\text{cl}}(t) = \lim_{J \rightarrow \infty} \frac{\langle \alpha | \hat{H}(t) | \alpha \rangle}{J}$; the resonant conditions are not modified by dividing the Hamiltonian by J , however the perturbation strength does change as $\epsilon \rightarrow \epsilon/J$. Consequently, the scalings obtained for ϵ_{\max} modify to $\epsilon_{\max}^{\text{NR}} \rightarrow AJ^0 = A$ (finite value) for non-resonant states and $\epsilon_{\max}^{\text{R}} \rightarrow BJ^{-1}$ or $CJ^{-3/2} \xrightarrow{J \rightarrow \infty} 0$ for resonant states, thus recovering the classical KAM theorem. Furthermore, the scalings can be justified by using unitary perturbation theory, from which, additionally, we can clearly identify the roles played by the matrix elements $\hat{K}_{k,k'} \equiv \langle E_k | \hat{K} | E_{k'} \rangle$ and the quantum resonant condition, Eq.(5).

Unitary perturbation theory.— Unitary perturbation theory (UPT) [36, 48] consists of expanding the Floquet quasienergies and (unnormalized) eigenfunctions in powers of the perturbation strength ϵ ,

$$\phi_k = \sum_{i=0} \phi_k^{(i)} \epsilon^i, \quad |f_k\rangle_u = \sum_{i=0} \epsilon^i |f_k^{(i)}\rangle. \quad (8)$$

By substituting these expressions in $\hat{F} |f_k\rangle_u = \exp(-i\phi_k) |f_k\rangle_u$, we obtain iteratively the different corrections to the Floquet eigenstates and quasienergies [63]. At order zero, the quasienergies are given by the eigen-phases of $\hat{F}_o = \exp(-i\tau \hat{H}_o)$, $\phi_k^{(0)} = \text{mod}(\tau E_k, 2\pi)$. Similar to standard perturbation theory, the calculation of the perturbative series differs in the degenerate case, which occurs in UPT when $\phi_k^{(0)} = \phi_{k'}^{(0)}$. Due to the modulo 2π , this condition implies $\tau(E_k - E_{k'}) = 2\pi n$, which is the exact quantum resonant condition in Eq. (5). Non-degenerate perturbation theory applies for non-resonant

states, as well as states close to quantum resonance, and degenerate perturbation theory is required to deal with exact quantum resonances.

In the non-degenerate case, after consistently normalizing the Floquet eigenfunctions, we obtain [63] a perturbative series for the maximum overlap of the Floquet eigenstates (7), $\mathcal{F}_{k,\max} = 1 - a_2\epsilon^2 - a_3\epsilon^3 - a_4\epsilon^4 - \dots$, where

$$a_2 = \langle f_k^{(1)} | f_k^{(1)} \rangle = \frac{1}{4} \sum_{l \neq k} \frac{|\langle E_l | \hat{K} | E_k \rangle|^2}{\sin^2\left(\frac{\tau(E_l - E_k)}{2}\right)}. \quad (9)$$

The matrix elements $\langle E_l | \hat{K} | E_k \rangle$, as shown in Fig.3(e), scale linearly with J , implying the numerators in (9) scale quadratically with J . Meanwhile, the denominators have relevant differences depending on whether the state is non-resonant or close to a resonance. Non-resonant states are free of small denominators, but for a state close to a resonance $m:n$, the argument of the sine function for $l = k + m$ is very close to a multiple of π : $\tau(E_{k+m} - E_k)/2 = n\pi + \delta$, where δ , as shown in Fig.3(d) ($\frac{\tau}{nT_{k,m}} = 1 + \frac{\delta}{\pi n}$), approaches zero as $\delta = \delta_{m:n}/J$. Consequently, this resonant sum term yields an additional J^2 scaling for a_2 , coming from $\frac{1}{\sin^2(\tau(E_{k+m} - E_k)/2)} \approx \frac{J^2}{\delta_{m:n}^2}$. Note that the intensity of a resonance is determined by the matrix element $\langle E_{k+m} | \hat{K} | E_k \rangle$, and that in order for the resonance to manifest, this matrix element must be non-zero. From the previous discussion, we obtain $a_2 = a_{2,\text{NR}}J^2$ for non-resonant states, whereas, for close-to-resonant states $a_2 = a_{2,\text{NR}}J^2 + a_{2,\text{CR}}J^4 \xrightarrow{J \rightarrow \infty} a_{2,\text{CR}}J^4$. Similarly, it can be shown [63] that for non-resonant states $a_3 \approx a_{3,\text{NR}}J^3$, whereas for states close to resonance the dominant behavior is $a_3 \approx a_{3,\text{CR}}J^6$. If for large enough J these scalings generalize to higher order perturbative terms $a_p = a_{p,\text{NR}}J^p$ and $a_p = a_{p,\text{CR}}J^{2p}$, the perturbative series for non-resonant and close to resonance states are, respectively,

$$\mathcal{F}_{k,\max}^{\text{NR}} \approx 1 - \sum_{p=2}^{p_o} a_{p,\text{NR}}(\epsilon J)^p \quad (10)$$

$$\mathcal{F}_{k,\max}^{\text{CR}} \approx 1 - \sum_{p=2}^{p_o} a_{p,\text{CR}}(\epsilon J^2)^p. \quad (11)$$

To determine ϵ_{\max} , we solve the equation $\mathcal{F}_{\max} = 1/2$, Eq. (7), for ϵ . By truncating the perturbative series until a certain power of ϵ , p_o , we are left with a polynomial equation in terms of variable $z = \epsilon J$ for non-resonant states and in terms of variable $z = \epsilon J^2$ for states close to resonance. Let z_{NR} and z_{CR} denote the respective physically meaningful solutions of these equations. Then, for non-resonant states, we obtain $\epsilon_{\max} = z_{\text{NR}}/J$, whereas for states close to resonance $\epsilon_{\max} = z_{\text{CR}}/J^2$, which are scalings very similar to those obtained numerically, shown in Fig.3(a)-(b).

For exact resonances, the degenerate subspace of \hat{F}_o is spanned by the states $|E_k\rangle$ and $|E_{k+m}\rangle$. The zeroth

order corrections to the Floquet eigenfunctions and first order corrections to the quasi-energies, $\phi_a^{(1)}$ are obtained from diagonalizing the kick operator in this subspace

$$\begin{pmatrix} \hat{K}_{k,k} & \hat{K}_{k,k+m} \\ \hat{K}_{k+m,k} & \hat{K}_{k+m,k+m} \end{pmatrix} \begin{pmatrix} c_{a,1} \\ c_{a,2} \end{pmatrix} = \phi_a^{(1)} \begin{pmatrix} c_{a,1} \\ c_{a,2} \end{pmatrix}, \quad (12)$$

with $a = k, k + m$ and, assuming $|c_{k,1}| > |c_{k,2}|$,

$$|f_k^{(0)}\rangle = c_{k,1}|E_k\rangle + c_{k,2}|E_{k+m}\rangle, \quad (13)$$

$$|f_{k+m}^{(0)}\rangle = c_{k+m,1}|E_k\rangle + c_{k+m,2}|E_{k+m}\rangle. \quad (14)$$

By analyzing the scaling of the matrix elements in (12), we obtain $c_{k,1} \approx \frac{1}{\sqrt{2}}(1 + \frac{\epsilon}{J})$ [63]. This implies that in the case of exact resonance, even for infinitesimal ϵ , the eigenstates of the Floquet operators are a linear combination of two eigenstates of \hat{H}_o with almost the same contribution from each. The perturbative expression for the maximum overlap until quadratic terms is now $\mathcal{F}_{k,\max}^{\text{ER}} = (1 - a_2^{\text{ER}}\epsilon^2)|c_{k,1}|^2$, where a_2^{ER} is given by the same expression as in Eq.(9) with $|E_k\rangle \rightarrow |f_k^{(0)}\rangle$ and the sum restriction now excluding the two states involved in the exact resonance ($\sum_{l \neq k, k+m}$), thus avoiding an ill-defined expression. From the scalings of the matrix elements and small denominators, we obtain $a_2^{\text{ER}} = a_{2,\text{ER}}J^4$, which implies $\mathcal{F}_{k,\max}^{\text{ER}} = \frac{1}{2} + \frac{\epsilon}{J} - \frac{a_{2,\text{ER}}}{2}J^4\epsilon^2$. Additionally, from $\mathcal{F}_{k,\max}^{\text{ER}} = \frac{1}{2}$, we deduce that $\epsilon_{\max} = \sqrt{\frac{2c}{a_{2,\text{ER}}}} \frac{1}{J^{5/2}}$, which coincides very well with the scaling obtained numerically as shown in Fig.3(c).

Concluding remarks.— By studying the eigenstates of the Floquet operator in terms of the eigenstates of the unperturbed Hamiltonian \hat{H}_0 , we have elucidated the mechanisms through which classical KAM resonances manifest in the quantum realm, in a kicked spin model for large but finite J . The results are expected to hold for a periodic driving in place of a periodic kick as the resonance conditions do not depend on the exact functional form of periodicity but only on the associated time period. We combine numerically exact results with analytical expressions obtained from unitary perturbation theory to derive the quantum precursors of KAM theorem. A potential application of our work is to provide a comprehensive framework that elucidates the effects of classical KAM resonances on quantum phenomena, such as measurement-induced transmon ionization. This has been explored in a recent study [68] where classical KAM resonances have been leveraged to explain the observed ionization in circuit quantum electrodynamics. Additionally, our framework could enhance the understanding of time crystals in the kicked LMG model [38, 39, 69] and other types of resonances in kicked systems [70–73]. The effect of resonances in the ground-state or, more generally, in states of \hat{H}_0 associated with classical fixed-points is an interesting extension of the study presented here.

ACKNOWLEDGMENTS

Acknowledgments.— MK, SH, and AST would like to thank Lauren Hayward and Ayana Sarkar for helpful discussions. MK acknowledges the support from the Applied Quantum Computing Challenge Program at the National Research Council of Canada. This research was supported in part by Perimeter Institute for Theoretical Physics. Research at Perimeter Institute is supported in part by the Government of Canada through the Department of Innovation, Science and Economic Development

and by the Province of Ontario through the Ministry of Colleges and Universities. JAS-L is grateful to the people of Mexico, who through Secretaría de Ciencias, Humanidades, Tecnología e Innovación (SECIHTI) funded his graduate education, CVU number:1181841. We acknowledge the support of the Computational Center ICN-UNAM, in particular to Enrique Palacios, Luciano Diaz, and Eduardo Murrieta. DJN acknowledges financial support from grant CZ.02.01.01/00/22_008/0004649 (QUEENTEC) provided by MEYS of the Czech Republic.

[1] K. Vogtmann, A. Weinstein, and V. Arnol'd, *Mathematical Methods of Classical Mechanics*, Graduate Texts in Mathematics (Springer New York, 1997).

[2] R. Livi, S. Ruffo, and D. Shepelyansky, Kolmogorov pathways from integrability to chaos and beyond, in *The Kolmogorov Legacy in Physics*, edited by R. Livi and A. Vulpiani (Springer Berlin Heidelberg, Berlin, Heidelberg, 2003) pp. 3–32.

[3] T. P. Weissert, The kolmogorov-arnold-moser theorem: “here comes the surprise”, in *The Genesis of Simulation in Dynamics: Pursuing the Fermi-Pasta-Ulam Problem* (Springer New York, New York, NY, 1997) pp. 51–82.

[4] S. PG, A. Sahu, N. D. Varikuti, B. K. Das, S. Manna, and V. Madhok, Information acquisition, scrambling, and sensitivity to errors in quantum chaos (2024), arXiv:2409.14332 [quant-ph].

[5] L. E. Reichl and W. A. Lin, The search for a quantum kam theorem, *Foundations of Physics* **17**, 689 (1987).

[6] G. P. Brandino, J.-S. Caux, and R. M. Konik, Glimmers of a quantum kam theorem: Insights from quantum quenches in one-dimensional bose gases, *Phys. Rev. X* **5**, 041043 (2015).

[7] D. Burgarth, P. Facchi, H. Nakazato, S. Pascazio, and K. Yuasa, Kolmogorov-arnold-moser stability for conserved quantities in finite-dimensional quantum systems, *Phys. Rev. Lett.* **126**, 150401 (2021).

[8] D. V. Kurlov, S. Malikis, and V. Gritsev, Quasiconserved quantities in the perturbed spin- $\frac{1}{2}$ xxx model, *Phys. Rev. B* **105**, 104302 (2022).

[9] P. Orlov, A. Tiutiakina, R. Sharipov, E. Petrova, V. Gritsev, and D. V. Kurlov, Adiabatic eigenstate deformations and weak integrability breaking of heisenberg chain, *Phys. Rev. B* **107**, 184312 (2023).

[10] W. Buijsman, V. Gritsev, and R. Sprik, Nonergodicity in the anisotropic dicke model, *Phys. Rev. Lett.* **118**, 080601 (2017).

[11] M. Pandey, P. W. Claeys, D. K. Campbell, A. Polkovnikov, and D. Sels, Adiabatic eigenstate deformations as a sensitive probe for quantum chaos, *Phys. Rev. X* **10**, 041017 (2020).

[12] B. Bertini, F. H. L. Essler, S. Groha, and N. J. Robinson, Thermalization and light cones in a model with weak integrability breaking, *Phys. Rev. B* **94**, 245117 (2016).

[13] A. A. Michailidis, C. J. Turner, Z. Papić, D. A. Abanin, and M. Serbyn, Slow quantum thermalization and many-body revivals from mixed phase space, *Phys. Rev. X* **10**, 011055 (2020).

[14] A. J. Friedman, S. Gopalakrishnan, and R. Vasseur, Diffusive hydrodynamics from integrability breaking, *Phys. Rev. B* **101**, 180302 (2020).

[15] A. Bastianello, A. De Luca, and R. Vasseur, Hydrodynamics of weak integrability breaking, *Journal of Statistical Mechanics: Theory and Experiment* **2021**, 114003 (2021).

[16] Y. Tang, W. Kao, K.-Y. Li, S. Seo, K. Mallayya, M. Rigol, S. Gopalakrishnan, and B. L. Lev, Thermalization near integrability in a dipolar quantum newton's cradle, *Phys. Rev. X* **8**, 021030 (2018).

[17] V. B. Bulchandani, D. A. Huse, and S. Gopalakrishnan, Onset of many-body quantum chaos due to breaking integrability, *Phys. Rev. B* **105**, 214308 (2022).

[18] V. A. Yurovsky, Exploring integrability-chaos transition with a sequence of independent perturbations, *Phys. Rev. Lett.* **130**, 020404 (2023).

[19] F. Haake, M. Kuš, and R. Scharf, Classical and quantum chaos for a kicked top, *Zeitschrift für Physik B Condensed Matter* 10.1007/BF01303727 (1987).

[20] M. H. Muñoz Arias, P. M. Poggi, and I. H. Deutsch, Nonlinear dynamics and quantum chaos of a family of kicked p -spin models, *Phys. Rev. E* **103**, 052212 (2021).

[21] S. Ray, A. Ghosh, and S. Sinha, Quantum signature of chaos and thermalization in the kicked dicke model, *Phys. Rev. E* **94**, 032103 (2016).

[22] M. Kumari and S. Ghose, Quantum-classical correspondence in the vicinity of periodic orbits, *Phys. Rev. E* **97**, 052209 (2018).

[23] S. Dogra, V. Madhok, and A. Lakshminarayanan, Quantum signatures of chaos, thermalization, and tunneling in the exactly solvable few-body kicked top, *Phys. Rev. E* **99**, 062217 (2019).

[24] U. T. Bhosale and M. S. Santhanam, Periodicity of quantum correlations in the quantum kicked top, *Phys. Rev. E* **98**, 052228 (2018).

[25] Q. Wang and M. Robnik, Power-law decay of the fraction of the mixed eigenstates in kicked top model with mixed-type classical phase space, *Phys. Rev. E* **108**, 054217 (2023).

[26] A. Anand, J. Davis, and S. Ghose, Quantum recurrences in the kicked top, *Phys. Rev. Res.* **6**, 023120 (2024).

[27] H. Sharma and U. T. Bhosale, Exactly solvable dynamics and signatures of integrability in an infinite-range many-body floquet spin system, *Phys. Rev. B* **109**, 014412 (2024).

[28] S. Sinha, S. Ray, and S. Sinha, Classical route to ergod-

icity and scarring in collective quantum systems, *Journal of Physics: Condensed Matter* **36**, 163001 (2024).

[29] X. Wang, S. Ghose, B. C. Sanders, and B. Hu, Entanglement as a signature of quantum chaos, *Phys. Rev. E* **70**, 016217 (2004).

[30] S. Ghose, R. Stock, P. Jessen, R. Lal, and A. Silberfarb, Chaos, entanglement, and decoherence in the quantum kicked top, *Phys. Rev. A* **78**, 042318 (2008).

[31] M. Kumari, *Quantum-Classical Correspondence and Entanglement in Periodically Driven Spin Systems*, Ph.D. thesis (2019).

[32] J. B. Ruebeck, J. Lin, and A. K. Pattanayak, Entanglement and its relationship to classical dynamics, *Phys. Rev. E* **95**, 062222 (2017).

[33] A. Leroose and S. Pappalardi, Bridging entanglement dynamics and chaos in semiclassical systems, *Phys. Rev. A* **102**, 032404 (2020).

[34] H. Sharma and U. T. Bhosale, Exact solvability of entanglement for arbitrary initial state in an infinite-range floquet system (2024), arXiv:2411.16670 [quant-ph].

[35] L. M. Sieberer, T. Olsacher, A. Elben, M. Heyl, P. Hauke, F. Haake, and P. Zoller, Digital quantum simulation, trotter errors, and quantum chaos of the kicked top, *npj Quantum Information* **5**, 78 (2019).

[36] K. Chinni, M. H. Muñoz Arias, I. H. Deutsch, and P. M. Poggi, Trotter errors from dynamical structural instabilities of floquet maps in quantum simulation, *PRX Quantum* **3**, 010351 (2022).

[37] M. H. Muñoz Arias, P. M. Poggi, P. S. Jessen, and I. H. Deutsch, Simulating nonlinear dynamics of collective spins via quantum measurement and feedback, *Phys. Rev. Lett.* **124**, 110503 (2020).

[38] A. Russomanno, F. Iemini, M. Dalmonte, and R. Fazio, Floquet time crystal in the lipkin-meshkov-glick model, *Phys. Rev. B* **95**, 214307 (2017).

[39] M. H. Muñoz Arias, K. Chinni, and P. M. Poggi, Floquet time crystals in driven spin systems with all-to-all p -body interactions, *Phys. Rev. Res.* **4**, 023018 (2022).

[40] S. Chaudhury, A. Smith, B. E. Anderson, S. Ghose, and P. S. Jessen, Quantum signatures of chaos in a kicked top, *Nature* **461**, 768 (2009).

[41] C. Neill, P. Roushan, M. Fang, Y. Chen, M. Kolodrubetz, Z. Chen, A. Megrant, R. Barends, B. Campbell, B. Chiaro, A. Dunsworth, E. Jeffrey, J. Kelly, J. Mutus, P. J. J. O’Malley, C. Quintana, D. Sank, A. Vainsencher, J. Wenner, T. C. White, A. Polkovnikov, and J. M. Martinis, Ergodic dynamics and thermalization in an isolated quantum system, *Nature Physics* **12**, 1037 (2016).

[42] V. R. Krithika, V. S. Anjusha, U. T. Bhosale, and T. S. Mahesh, Nmr studies of quantum chaos in a two-qubit kicked top, *Phys. Rev. E* **99**, 032219 (2019).

[43] D. A. Wisniacki, M. Saraceno, F. J. Arranz, R. M. Benito, and F. Borondo, Poincaré-birkhoff theorem in quantum mechanics, *Phys. Rev. E* **84**, 026206 (2011).

[44] T. P. Billam and S. A. Gardiner, Quantum resonances in an atom-optical δ -kicked harmonic oscillator, *Phys. Rev. A* **80**, 023414 (2009).

[45] D. A. Wisniacki and P. Schlagheck, Quantum manifestations of classical nonlinear resonances, *Phys. Rev. E* **92**, 062923 (2015).

[46] G. Floquet, Sur les équations différentielles linéaires à coefficients périodiques, *Annales scientifiques de l’École Normale Supérieure 2e série*, **12**, 47 (1883).

[47] M. Grifoni and P. Hänggi, Driven quantum tunneling, *Physics Reports* **304**, 229 (1998).

[48] A. Peres, *Quantum Theory: Concepts and Methods*, 1st ed. (Springer Dordrecht, 1993) available online: <https://link.springer.com/book/10.1007/0-306-47120-5>.

[49] M. Bukov, M. Heyl, D. A. Huse, and A. Polkovnikov, Heating and many-body resonances in a periodically driven two-band system, *Phys. Rev. B* **93**, 155132 (2016).

[50] P. W. Claeys, S. De Baerdemacker, O. E. Araby, and J.-S. Caux, Spin polarization through floquet resonances in a driven central spin model, *Phys. Rev. Lett.* **121**, 080401 (2018).

[51] S. J. Garratt, S. Roy, and J. T. Chalker, Local resonances and parametric level dynamics in the many-body localized phase, *Phys. Rev. B* **104**, 184203 (2021).

[52] A. Morningstar, L. Colmenarez, V. Khemani, D. J. Luitz, and D. A. Huse, Avalanches and many-body resonances in many-body localized systems, *Phys. Rev. B* **105**, 174205 (2022).

[53] J. A. Segura-Landa, M. Kumari, D. Julian Nader, S. Husnugil, A. SaraerToosi, and S. Lerma-Hernandez, Quantum precursors to kolmogorov-arnold-moser theorem in floquet spin-j systems, 10.5281/zenodo.15360343 (2025).

[54] L. Landau and E. Lifshitz, *Quantum Mechanics: Non-Relativistic Theory*, Course of theoretical physics (Elsevier, 1991) Chap. §48.

[55] H. Lipkin, N. Meshkov, and A. Glick, Validity of many-body approximation methods for a solvable model: (i). exact solutions and perturbation theory, *Nuclear Physics* **62**, 188 (1965).

[56] D. J. Nader, C. A. González-Rodríguez, and S. Lerma-Hernández, Avoided crossings and dynamical tunneling close to excited-state quantum phase transitions, *Phys. Rev. E* **104**, 064116 (2021).

[57] O. Castaños, R. López-Peña, J. G. Hirsch, and E. López-Moreno, Classical and quantum phase transitions in the lipkin-meshkov-glick model, *Phys. Rev. B* **74**, 104118 (2006).

[58] P. Ribeiro, J. Vidal, and R. Mosseri, Exact spectrum of the lipkin-meshkov-glick model in the thermodynamic limit and finite-size corrections, *Phys. Rev. E* **78**, 021106 (2008).

[59] J. A. Segura Landa, *Quantum KAM resonances*, Master’s thesis, Universidad Veracruzana. Facultad de Física. Región Xalapa (2024).

[60] P. Cejnar, P. Stránský, M. Macek, and M. Kloc, Excited-state quantum phase transitions, *Journal of Physics A: Mathematical and Theoretical* **54**, 133001 (2021).

[61] A. D. Ribeiro, M. A. M. de Aguiar, and A. F. R. de Toledo Piza, The semiclassical coherent state propagator for systems with spin, *Journal of Physics A: Mathematical and General* **39**, 3085 (2006).

[62] P. Ribeiro, J. Vidal, and R. Mosseri, Exact spectrum of the lipkin-meshkov-glick model in the thermodynamic limit and finite-size corrections, *Phys. Rev. E* **78**, 021106 (2008).

[63] See supplemental material, URL_will_be_inserted_by_publisher.

[64] W. Beugeling, A. Andrianov, and M. Haque, Global characteristics of all eigenstates of local many-body hamiltonians: participation ratio and entanglement entropy, *Journal of Statistical Mechanics: Theory and Experiment* **2015**, P02002 (2015).

[65] M. Gonzalez, M. A. Bastarrachea-Magnani, and J. G.

Hirsch, Phase space geometry of collective spin systems: Scaling and fractality (2025), arXiv:2502.15169 [quant-ph].

[66] L. Reichl, Time-periodic quantum systems, in *The Transition to Chaos: Conservative Classical and Quantum Systems* (Springer International Publishing, Cham, 2021) pp. 339–396.

[67] G. Hose and H. S. Taylor, Quantum kolmogorov-arnol'd-moser-like theorem: Fundamentals of localization in quantum theory, *Phys. Rev. Lett.* **51**, 947 (1983).

[68] M. F. Dumas, B. Groleau-Paré, A. McDonald, M. H. Muñoz Arias, C. Lledó, B. D'Anjou, and A. Blais, Measurement-induced transmon ionization, *Phys. Rev. X* **14**, 041023 (2024).

[69] M. P. Zaletel, M. Lukin, C. Monroe, C. Nayak, F. Wilczek, and N. Y. Yao, Colloquium: Quantum and classical discrete time crystals, *Rev. Mod. Phys.* **95**, 031001 (2023).

[70] N. D. Varikuti, A. Sahu, A. Lakshminarayan, and V. Madhok, Probing dynamical sensitivity of a non-kolmogorov-arnold-moser system through out-of-time-order correlators, *Phys. Rev. E* **109**, 014209 (2024).

[71] H. Wang, J. Wang, I. Guarneri, G. Casati, and J. Gong, Exponential quantum spreading in a class of kicked rotor systems near high-order resonances, *Phys. Rev. E* **88**, 052919 (2013).

[72] V. Ramareddy, G. Behinaein, I. Talukdar, P. Ahmadi, and G. S. Summy, High-order resonances of the quantum δ -kicked accelerator, *Europhysics Letters* **89**, 33001 (2010).

[73] V. V. Sokolov, O. V. Zhirov, D. Alonso, and G. Casati, Quantum resonances of the kicked rotor and the $SU(q)$ group, *Phys. Rev. Lett.* **84**, 3566 (2000).

Supplemental Material: Quantum precursors to Kolmogorov-Arnold-Moser theorem in Floquet spin- J systems

Jesús A. Segura-Landa ^{1,2}, Meenu Kumari^{3,4}, Daniel J. Nader⁵,

Sercan Hüsnügil^{4,6}, Ali SaraerToosi^{4,7}, and Sergio Lerma-Hernández¹

¹Facultad de Física, Universidad Veracruzana, Campus Arco Sur, Paseo 112, C.P. 91097 Xalapa, Mexico.

²Instituto de Ciencias Nucleares, Universidad Nacional Autónoma de México,

Apdo. Postal 70-543, C.P. 04510 Cd. Mx., Mexico

³Digital Technologies, National Research Council Canada

⁴Perimeter Institute for Theoretical Physics, Waterloo ON N2L 2Y5, Canada

⁵Department of Optics, Faculty of Science, Palacky University, Olomouc, 77900, Czech Republic

⁶Department of Physics and Astronomy, University of Waterloo, Waterloo, Ontario, N2L 3G1, Canada and

⁷Department of Computer Science, University of Toronto,

40 St. George St., Toronto, ON, M5S 2E4, Canada

CONTENTS

I. Nonlinear resonances and classical time period	1
II. Participation ratio for exact quantum resonances	2
III. Unitary perturbation theory	3
A. Non-degenerate case	4
B. Degenerate case	5
IV. Perturbative series for \mathcal{F}_{\max} : non-resonant and close-to-resonance cases	6
A. Second order term a_2	6
B. Third order term a_3	8
C. Scaling of ϵ_{\max} from the perturbative series	10
D. Dominance of the largest power of J in the coefficients of the $\mathcal{F}_{k,\max}$ perturbative series	12
V. Perturbative series for \mathcal{F}_{\max} : exact resonance case	14
A. Dependence on J of $\langle E_a f_a^{(0)} \rangle$ and $\langle E_a f_{a'}^{(0)} \rangle$	15
B. Dependence on J of $\langle f_{a'}^{(0)} f_a^{(1)} \rangle$	16
C. Scaling of ϵ_{\max} for exact resonances	17

I. NONLINEAR RESONANCES AND CLASSICAL TIME PERIOD

In classical physics, all time-independent Hamiltonians with one degree of freedom are integrable, thus expressible as $h_o = h_o(I)$ in the action-angle variable form. Hence, we study a one-degree-of-freedom time-periodic Hamiltonian to explore integrability breaking, given by:

$$h(I, \theta, t) = h_o(I) + \epsilon k(I, \theta, t), \quad \epsilon \ll 1, \quad (\text{S.1})$$

where $h_o(I)$ represents the integrable Hamiltonian with action-angle variables (I, θ) and $k(I, \theta, \tau)$ is a time-periodic perturbing Hamiltonian with period τ , i.e., $k(I, \theta, t + \tau) = k(I, \theta, t)$. For the integrable Hamiltonian considered in the main text, the classical hamiltonian is obtained from Bloch coherent states, $|\alpha\rangle$, as

$$h_o(\phi, z_c) \equiv \lim_{J \rightarrow \infty} \frac{\langle \alpha | \hat{H}_0 | \alpha \rangle}{J} = z_c + \frac{(1 - z_c^2)}{2} [\gamma_x \cos^2 \phi + \gamma_y \sin^2 \phi], \quad (\text{S.2})$$

where $\langle \alpha | \hat{J}_z | \alpha \rangle / J = z_c$, $\langle \alpha | \hat{J}_x | \alpha \rangle / J = \sqrt{1 - z_c^2} \cos \phi$ and $\langle \alpha | \hat{J}_y | \alpha \rangle / J = \sqrt{1 - z_c^2} \sin \phi$. The action of the torus with the rescaled energy $\varepsilon \equiv E/J$ is defined as $I = \frac{1}{2\pi} \oint z_c(\varepsilon, \phi) d\phi$. Here we have used the canonical coordinates

(ϕ, z_c) , which are related to the canonical coordinates used in main text, (Q, P) , through $Q = \sqrt{2(1+z_c)} \cos \phi$ and $P = -\sqrt{2(1+z_c)} \sin \phi$. A resonance between the time degree of freedom of $k(I, \theta, t)$ and the degree of freedom of h_o occurs whenever the driving frequency of the perturbing Hamiltonian $\omega = 2\pi/\tau$ matches a rational multiple of the natural frequency of h_o , given by $\Omega(I) = dh_o/dI$:

$$m\Omega_{m:n} = n\omega, \quad \Omega_{m:n} = \left. \left(\frac{dh_o}{dI} \right) \right|_{I=I_{m:n}}, \quad m, n \in \mathbb{Z}, \quad (\text{S.3})$$

where $I_{m:n}$ is the action of the torus whose frequency is associated with the $m:n$ resonance. For a tori with energy ε in the classical phase space of h_o , the time period $T(\varepsilon)$ of the tori is given by (note that all tori of $h_o(I)$ are closed orbits):

$$T(\varepsilon) = \frac{2\pi}{\Omega(\varepsilon)} = 2\pi \frac{dI(\varepsilon)}{d\varepsilon}. \quad (\text{S.4})$$

In terms of time periods, the resonant condition (S.3) is written as

$$m\tau = nT(I_{m:n}), \quad (\text{S.5})$$

and it generates an m -cycle in the stroboscopic dynamics in the phase space. The classical time period for an orbit of energy ε of the Hamiltonian (S.2) is obtained from the following integral

$$T(\varepsilon) = \int_0^{2\pi} \frac{d\phi}{\sqrt{1 - 2\varepsilon A(\phi) + A(\phi)^2}}, \quad (\text{S.6})$$

where $A(\phi) = \gamma_x \cos^2(\phi) + \gamma_y \sin^2(\phi)$. For the parameters used in the main text, $\gamma_y = 0$ and $\gamma_x = -0.95$, it reduces to $A(\phi) = -0.95 \cos^2(\phi)$. The general expression for the classical LMG Hamiltonian can be found in Ref. [56] of main text. For the time-dependence of $k(I, \theta, \tau)$, we choose time-periodic delta function, $\delta(t - n\tau)$, $n \in \mathbb{Z}$ which makes the analytical calculations for the model in quantum physics possible using unitary perturbation theory. As the time-periodic delta function imparts a periodic kick to the system, we refer to the driving time period and driving frequency as kicking period and kicking frequency, respectively.

II. PARTICIPATION RATIO FOR EXACT QUANTUM RESONANCES

The participation ratio (PR) of normalized Floquet eigenstates, $|f_k\rangle$, in the unperturbed Hamiltonian eigenbasis, $|E_n\rangle$, is defined as

$$\text{PR} \equiv \left(\sum_{n=1}^N |\langle E_n | f_k \rangle|^4 \right)^{-1}, \quad (\text{S.7})$$

where N is the Hilbert space dimension (for pseudo-spin systems, $N = 2J+1$). Also referred as the number of principal components (NPC) in literature [18], the PR measures how extensively the state $|f_k\rangle$ is spread in the eigenbasis $|E_n\rangle$. Its minimum value is equal to 1 when $|f_k\rangle$ coincides with a single state of the basis $|E_n\rangle$, and maximum value is N when $|f_k\rangle$ is evenly distributed across all the elements of the eigenbasis $|E_n\rangle$. In contrast, the inverse of the Participation Ratio (IPR), defined as $\text{IPR} = 1/\text{PR}$, is maximal (equal to 1) when the state is maximally localized, and minimal (equal to 1/N) when the state is fully delocalized.

The PR is highly sensitive to the proximity of resonances, showing sharp peaks for states close to resonances (as shown in Fig. 1(b) of main text where $\ln(\text{PR})$ is plotted for $|f_k\rangle$), as well as for states involved in exact quantum resonances. States involved in exact quantum resonances show a pronounced increase of the PR, as shown in Fig. S.1, where we plot the PR for close-to-resonance (CR) states (orange) and exact resonance (ER) states (blue) for resonances 1:1, 2:1, 2:3, 3:4, 3:5 and 4:5. While the kicking period was fixed for all the CR states to $\tau = 8$, this period was fine-tuned for the case of ER states as mentioned in the figures. In all cases, the exact resonant condition considerably increases the PR of resonant states, indicating greater delocalization of the involved states.

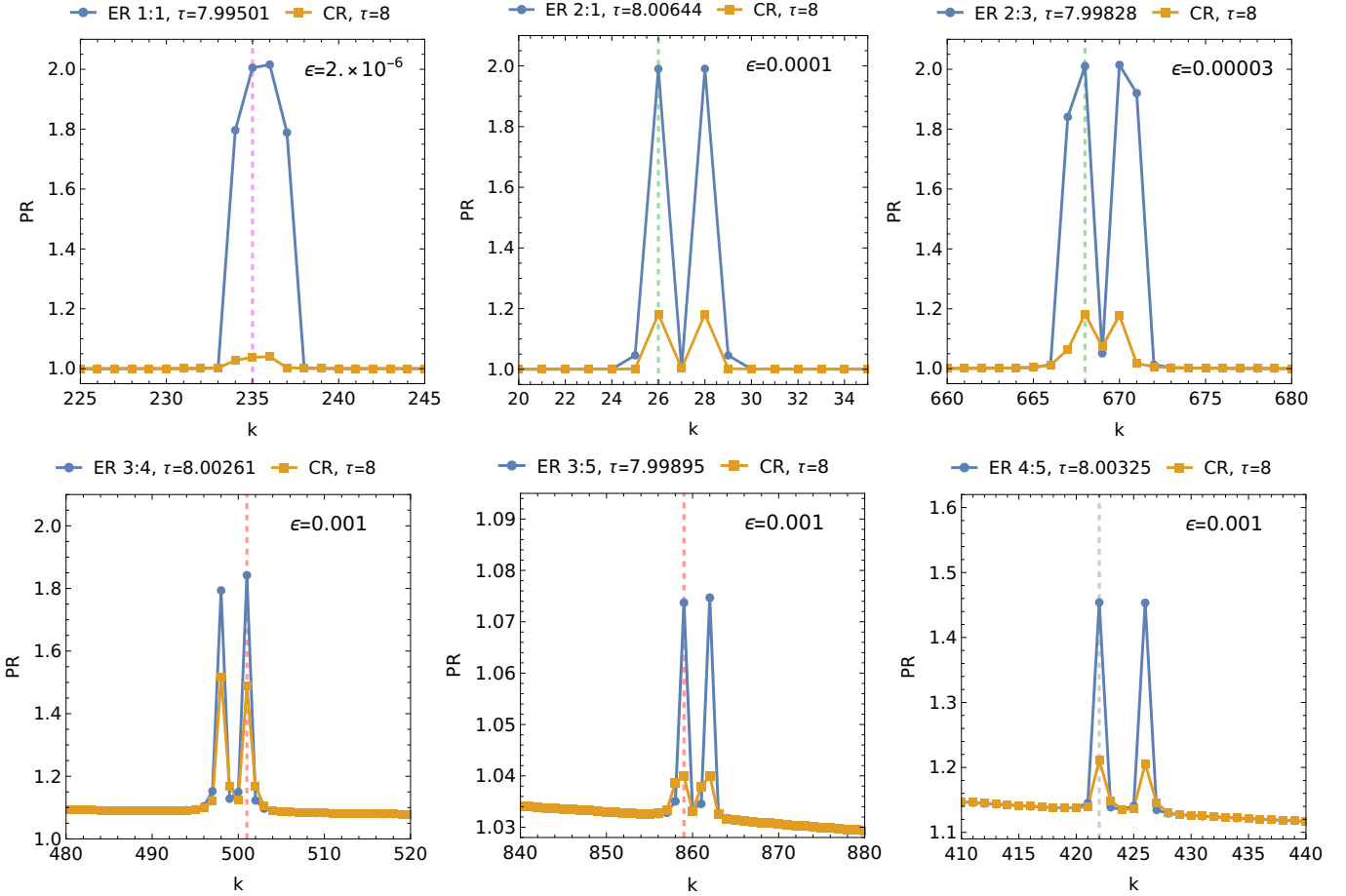


FIG. S.1. Participation ratio (PR) of the Floquet eigenstates, $|f_k\rangle$, in the energy eigenbasis, $|E_n\rangle$ of the LMG model. The top row shows PR for resonances 1:1, 2:1 and 2:3 from left to right. The bottom row shows PR for resonances 3:4, 3:5 and 4:5. In all cases, $J = 500$, blue data points indicate the PR for exact quantum resonances (with the kicking period adjusted for each case), and orange data points represent approximate quantum resonance with $\tau = 8$. The perturbation strength, ϵ , of the kick is specified in each plot.

III. UNITARY PERTURBATION THEORY

In this section, we review the unitary perturbation theory [48] and present expressions for the lower-order corrections. Similar to standard perturbation theory, we distinguish between non-degenerate and degenerate cases.

Unitary perturbation theory enables us to derive approximate expressions for Floquet eigenstates and quasienergies provided that the Floquet operator \hat{F} can be expressed as a product of two unitaries: $\hat{F} = \hat{F}_0 \hat{F}_K = \exp(-i\tau \hat{H}_0) \exp(-i\epsilon \hat{K})$. This form arises when the time-dependence in the perturbing Hamiltonian is a periodic delta function. It also requires the knowledge of the eigenfunctions and eigenvalues of \hat{H}_0 , $\hat{H}_0|E_k\rangle = E_k|E_k\rangle$ with $\langle E_{k'}|E_k\rangle = \delta_{k'k}$. Consequently, $\hat{F}_0|E_k\rangle = \exp(-i\tau E_k)|E_k\rangle = \exp[-i \text{mod}(\tau E_k, 2\pi)]|E_k\rangle$. To obtain the approximate expressions, the quasienergies and Floquet eigenstates are expanded in powers of ϵ :

$$\phi_k = \sum_{i=0} \phi_k^{(i)} \epsilon^i = \phi_k^{(0)} + \epsilon \phi_k^{(1)} + \epsilon^2 \phi_k^{(2)} + \dots \quad (\text{S.8})$$

$$|f_k\rangle_u = \sum_{i=0} \epsilon^i |f_k^{(i)}\rangle = |f_k^{(0)}\rangle + \epsilon |f_k^{(1)}\rangle + \epsilon^2 |f_k^{(2)}\rangle + \dots \quad (\text{S.9})$$

We consider that the zero-order corrections form an orthonormal basis, $\langle f_{k'}^{(0)}|f_k^{(0)}\rangle = \delta_{k'k}$, and without loss of generality it can be assumed that the higher order corrections are orthogonal to them, $\langle f_k^{(0)}|f_k^{(i)}\rangle = 0$ for $i \geq 1$. These

assumptions imply that the eigenfunctions $|f_k\rangle_u$ are unnormalized. Normalized eigenfunctions can be obtained by expanding consistently in powers of ϵ , $|f_k\rangle = Z|f_k\rangle_u$, where the normalization constant is $Z = \frac{1}{\sqrt{u\langle f_k|f_k\rangle_u}}$.

After expanding \hat{F} in powers of ϵ , we substitute the perturbative series into the equation $\hat{F}|f_k\rangle_u = \exp(-i\phi_k)|f_k\rangle_u$,

$$e^{-i\hat{H}_0\tau} \left(|f_k^{(0)}\rangle + \epsilon \left[|f_k^{(1)}\rangle - i\hat{K}|f_k^{(0)}\rangle \right] + \epsilon^2 \left[|f_k^{(2)}\rangle - i\hat{K}|f_k^{(1)}\rangle - \frac{1}{2}\hat{K}^2|f_k^{(0)}\rangle \right] + \dots \right) = \quad (\text{S.10})$$

$$e^{-i\phi_k^{(0)}} \left(|f_k^{(0)}\rangle + \epsilon \left[|f_k^{(1)}\rangle - i\phi_k^{(1)}|f_k^{(0)}\rangle \right] + \epsilon^2 \left[|f_k^{(2)}\rangle - i\phi_k^{(1)}|f_k^{(1)}\rangle - \left\{ i\phi_k^{(2)} + \frac{1}{2}(\phi_k^{(1)})^2 \right\} |f_k^{(0)}\rangle \right] + \dots \right).$$

In this way, we obtain a set of equations by equating the terms with the same power of ϵ . Then, we use the resulting equations to obtain iteratively the successive corrections to the quasienergies and Floquet eigenstates, as we explain in the following subsections for the non-degenerate and degenerate cases, respectively.

A. Non-degenerate case

For an eigenstate of $\hat{F}_0 = e^{-i\hat{H}_0\tau}$, whose quasienergy is non-degenerate, $\phi_k^{(0)} = \text{mod}(\tau E_k, 2\pi) \neq \text{mod}(\tau E_{k'}, 2\pi)$ for $k' \neq k$, which is the case for non-resonant states and also for close-to-resonance quantum states, the zero-order equation,

$$e^{-i\hat{H}_0\tau}|f_k^{(0)}\rangle = e^{-i\phi_k^{(0)}}|f_k^{(0)}\rangle,$$

implies that $|f_k^{(0)}\rangle = |E_k\rangle$. From this, the first order equation becomes

$$e^{-i\hat{H}_0\tau} \left[|f_k^{(1)}\rangle - i\hat{K}|E_k\rangle \right] = e^{-iE_k\tau} \left[|f_k^{(1)}\rangle - i\phi_k^{(1)}|E_k\rangle \right].$$

We multiply this equation by $\langle E_k|$, and use $\langle E_k|f_k^{(1)}\rangle = 0$ and $\langle E_k|E_k\rangle = 1$ to obtain $\phi_k^{(1)} = \langle E_k|\hat{K}|E_k\rangle$. The first order correction to the Floquet eigenstates are obtained from multiplying the same equation but now by $\langle E_{k'}|$ with $k' \neq k$,

$$(e^{-iE_{k'}\tau} - e^{-iE_k\tau}) \langle E_{k'}|f_k^{(1)}\rangle = ie^{-iE_{k'}\tau} \langle E_{k'}|\hat{K}|E_k\rangle. \quad (\text{S.11})$$

From this, we obtain the components of the first order correction to the Floquet eigenstates in the \hat{H}_0 eigenbasis, $\langle E_{k'}|f_k^{(1)}\rangle$. By repeating this procedure for higher order equations, we obtain the corrections to the quasienergies

$$\phi_k^{(0)} = E_k\tau \quad (\text{S.12})$$

$$\phi_k^{(1)} = \langle E_k|\hat{K}|E_k\rangle \quad (\text{S.13})$$

$$\phi_k^{(2)} = \langle E_k|\hat{K}|f_k^{(1)}\rangle - \frac{i}{2}\langle E_k|\hat{K}^2|E_k\rangle + \frac{i}{2}(\phi_k^{(1)})^2 = \frac{1}{2} \sum_{k' \neq k} \cot \left[\frac{\tau(E_k - E_{k'})}{2} \right] \left| \langle E_k|\hat{K}|E_{k'}\rangle \right|^2 \quad (\text{S.14})$$

$$\phi_k^{(3)} = i\phi_k^{(1)}\phi_k^{(2)} + \frac{1}{6}(\phi_k^{(1)})^3 + \langle E_k|\hat{K}|f_k^{(2)}\rangle - \frac{i}{2}\langle E_k|\hat{K}^2|f_k^{(1)}\rangle - \frac{1}{6}\langle E_k|\hat{K}^3|E_k\rangle. \quad (\text{S.15})$$

Subsequent to the quasienergy corrections, the components of the corrections to the unnormalized Floquet eigenfunctions, in the \hat{H}_0 eigenbasis, are given by ($k' \neq k$ for corrections of order $i \geq 1$)

$$\langle E_{k'}|f_k^{(0)}\rangle = \delta_{k'k} \quad (\text{S.16})$$

$$\langle E_{k'}|f_k^{(1)}\rangle = -i \frac{\langle E_{k'}|\hat{K}|E_k\rangle}{e^{i\tau(E_{k'}-E_k)} - 1} \quad (\text{S.17})$$

$$\left(e^{i\tau(E_{k'}-E_k)} - 1 \right) \langle E_{k'}|f_k^{(2)}\rangle = -i\langle E_{k'}|\hat{K}|f_k^{(1)}\rangle - \frac{1}{2}\langle E_{k'}|\hat{K}^2|E_k\rangle + ie^{i\tau(E_{k'}-E_k)}\phi_k^{(1)}\langle E_{k'}|f_k^{(1)}\rangle \quad (\text{S.18})$$

$$\left(e^{i\tau(E_{k'}-E_k)} - 1 \right) \langle E_{k'}|f_k^{(3)}\rangle = -i\langle E_{k'}|\hat{K}|f_k^{(2)}\rangle - \frac{1}{2}\langle E_{k'}|\hat{K}^2|f_k^{(1)}\rangle + \frac{i}{6}\langle E_{k'}|\hat{K}^3|E_k\rangle + e^{i\tau(E_{k'}-E_k)} \left(i\phi_k^{(1)}\langle E_{k'}|f_k^{(2)}\rangle + \left[i\phi_k^{(2)} + \frac{1}{2}(\phi_k^{(1)})^2 \right] \langle E_{k'}|f_k^{(1)}\rangle \right). \quad (\text{S.19})$$

Moreover, if the state $|E_k\rangle$ satisfies an exact quantum resonant condition $\tau(E_{k'} - E_k) = 2\pi n$, where $n \in \mathbb{Z}$ and $k' \neq k$, the previous expressions contain ill-defined terms. As is done in standard perturbation theory, a modified version of the perturbative expressions must be used in this scenario, which is discussed in the following subsection.

B. Degenerate case

In unitary perturbation theory, we have a degeneracy when two (or more) quasienergies of \hat{F}_0 are equal, $\phi_k^{(0)} = \text{mod}(\tau E_k, 2\pi) = \phi_{k'}^{(0)} = \text{mod}(\tau E_{k'}, 2\pi)$, for $k' \neq k$. Note that this can happen even when the spectrum of \hat{H}_0 is non-degenerate.

Suppose a two-fold degeneracy between states $|E_k\rangle$ and $|E_{k+m}\rangle$, and $\phi_k^{(0)} = \text{mod}(E_k\tau, 2\pi) = \text{mod}(E_{k+m}\tau, 2\pi) = \phi_{k+m}^{(0)}$. Due to the modulo 2π , we have a degeneracy for states $|E_k\rangle$ and $|E_{k+m}\rangle$ if

$$\tau(E_{k+m} - E_k) = 2\pi n, \quad n \in \mathbb{Z},$$

which is the resonant condition discussed in the main text, Eq. (5). Then, from the zero-order equation of Eq. (S.10),

$$e^{-i\hat{H}_0\tau}|f_a^{(0)}\rangle = e^{-i\phi_a^{(0)}}|f_a^{(0)}\rangle,$$

with $a = k, k + m$, we have two orthonormal states

$$|f_k^{(0)}\rangle = c_{k,1}|E_k\rangle + c_{k,2}|E_{k+m}\rangle \quad (\text{S.20})$$

$$|f_{k+m}^{(0)}\rangle = c_{k+m,1}|E_k\rangle + c_{k+m,2}|E_{k+m}\rangle, \quad (\text{S.21})$$

where the coefficients $c_{a,i}$ have to be determined, but in order to label the states $|f_a^{(0)}\rangle$, we have assumed that $|c_{k,1}| \geq |c_{k,2}|$, which implies $|c_{k+m,1}| \leq |c_{k+m,2}|$ because of orthogonality of $|f_k^{(0)}\rangle$ and $|f_{k+m}^{(0)}\rangle$. From the first order equation of Eq. (S.10),

$$e^{-i\hat{H}_0\tau} \left[|f_a^{(1)}\rangle - i\hat{K}|f_a^{(0)}\rangle \right] = e^{-i\phi_a\tau} \left[|f_a^{(1)}\rangle - i\phi_a^{(1)}|f_a^{(0)}\rangle \right], \quad (\text{S.22})$$

we obtain, after multiplying it by $\langle f_a^{(0)}|$,

$$\phi_a^{(1)} = \langle f_a^{(0)}|\hat{K}|f_a^{(0)}\rangle. \quad (\text{S.23})$$

On the other hand, if we now multiply Eq. (S.22) by $\langle \phi_{a'}^{(0)}|$, with $a' = k, k + m, a' \neq a$, we obtain

$$\langle f_{a'}^{(0)}|\hat{K}|f_a^{(0)}\rangle = ie^{i\phi_{a'}} \left(e^{-i\phi_a^{(0)}} - e^{-i\phi_{a'}^{(0)}} \right) \langle f_{a'}^{(0)}|f_a^{(1)}\rangle = 0, \quad (\text{S.24})$$

where in the last equality we have used the degeneracy $\phi_a^{(0)} = \phi_{a'}^{(0)}$. Eqs. (S.23) and (S.24) imply that the zeroth order eigenfunctions of the Floquet operator and first order corrections to the quasienergies are obtained from diagonalizing the perturbation \hat{K} in the degenerate subspace, i.e., from the normalized eigenvectors of the hermitian matrix

$$\begin{pmatrix} \langle E_k|\hat{K}|E_k\rangle & \langle E_k|\hat{K}|E_{k+m}\rangle \\ \langle E_{k+m}|\hat{K}|E_k\rangle & \langle E_{k+m}|\hat{K}|E_{k+m}\rangle \end{pmatrix} \begin{pmatrix} c_{a,1} \\ c_{a,2} \end{pmatrix} = \phi_a^{(1)} \begin{pmatrix} c_{a,1} \\ c_{a,2} \end{pmatrix}, \quad (\text{S.25})$$

where $a = k, k + m$ and the coefficients $c_{a,i}$ determine $|f_a^{(0)}\rangle$ according to Eqs. (S.20) and (S.21).

The components of the first-order correction to the unnormalized eigenfunctions, $|f_a\rangle_u$, in the \hat{H}_0 eigenbasis for $k' \neq k, k + m$ are obtained from multiplying Eq. (S.22) by the bra $\langle E_{k'}|$

$$\langle E_{k'}|f_a^{(1)}\rangle = -i \frac{\langle E_{k'}|\hat{K}|f_a^{(0)}\rangle}{e^{i\tau(E_{k'}-E_a)} - 1} \quad \text{for } k' \neq k, k + m. \quad (\text{S.26})$$

It remains to calculate the component of the first order correction in the degenerate subspace, $\langle f_{a'}^{(0)}|f_a^{(1)}\rangle$ for $a, a' = k$ or $k + m$ ($a' \neq a$). This component is obtained from the ϵ^2 terms in Eq. (S.10),

$$\begin{aligned} e^{-i\hat{H}_0\tau} \left[|f_a^{(2)}\rangle - i\hat{K}|f_a^{(1)}\rangle - \frac{1}{2}\hat{K}^2|f_a^{(0)}\rangle \right] = \\ e^{-i\phi_a^{(0)}} \left[|f_a^{(2)}\rangle - i\phi_a^{(1)}|f_a^{(1)}\rangle - \left\{ i\phi_a^{(2)} + \frac{1}{2}(\phi_a^{(1)})^2 \right\} |f_a^{(0)}\rangle \right]. \end{aligned} \quad (\text{S.27})$$

After multiplying it by $\langle f_{a'}^{(0)} |$ with $a' \neq a$, using the degeneracy condition, $\phi_{a'}^{(0)} = \phi_a^{(0)}$, and the orthogonality $\langle f_{a'}^{(0)} | f_a^{(0)} \rangle = 0$, we obtain

$$\phi_a^{(1)} \langle f_{a'}^{(0)} | f_a^{(1)} \rangle = \langle f_{a'}^{(0)} | \hat{K} | f_a^{(1)} \rangle - \frac{i}{2} \langle f_{a'}^{(0)} | \hat{K}^2 | f_a^{(0)} \rangle.$$

Then, we use the resolution of the identity $\mathbf{1} = \sum_{k' \neq k, k+m} |E_{k'}\rangle \langle E_{k'}| + |f_a^{(0)}\rangle \langle f_a^{(0)}| + |f_{a'}^{(0)}\rangle \langle f_{a'}^{(0)}|$ in the first term of the RHS of the previous equation to get

$$\phi_a^{(1)} \langle f_{a'}^{(0)} | f_a^{(1)} \rangle = \langle f_{a'}^{(0)} | \hat{K} | f_a^{(0)} \rangle \langle f_{a'}^{(0)} | f_a^{(1)} \rangle + \sum_{k' \neq k, k+m} \langle f_{a'}^{(0)} | \hat{K} | E_{k'} \rangle \langle E_{k'} | f_a^{(1)} \rangle - \frac{i}{2} \langle f_{a'}^{(0)} | \hat{K}^2 | f_a^{(0)} \rangle,$$

where we have used $\langle f_{a'}^{(0)} | \hat{K} | f_a^{(0)} \rangle = 0$. Finally, substituting Eqs.(S.23) and (S.26) in the previous equation, we obtain

$$\langle f_{a'}^{(0)} | f_a^{(1)} \rangle = -\frac{i}{\phi_a^{(1)} - \phi_{a'}^{(1)}} \left(\sum_{k' \neq k, k+m} \frac{\langle f_{a'}^{(0)} | \hat{K} | E_{k'} \rangle \langle E_{k'} | \hat{K} | f_a^{(0)} \rangle}{e^{i\tau(E_{k'} - E_a)} - 1} + \frac{1}{2} \langle f_{a'}^{(0)} | \hat{K}^2 | f_a^{(0)} \rangle \right). \quad (\text{S.28})$$

Higher order corrections can be obtained similarly, but for our purposes these corrections are sufficient.

Similar to the corrections for the non-degenerate case, the expressions for this degenerate case may have small denominators, as discussed in detail in Sec.V, but in contrast to the non-degenerate case, the previous expressions have no ill-defined terms when the resonant condition is exactly fulfilled.

IV. PERTURBATIVE SERIES FOR \mathcal{F}_{\max} : NON-RESONANT AND CLOSE-TO-RESONANCE CASES

In this section, we derive the perturbative series of $\mathcal{F}_{k,\max}$ for a non-degenerate case and determine the scaling of its terms with respect to the system size, J . This analysis allows us to establish the scaling of ϵ_{\max} for non-resonant and close-to-resonance cases, as discussed in the main text.

For small ϵ in unitary perturbation theory, the maximum overlap of the Floquet eigenstates with respect to the \hat{H}_0 eigenbasis, $\mathcal{F}_{k,\max} \equiv \max_n |\langle f_k | E_n \rangle|^2$ is simply given by $\mathcal{F}_{k,\max} = |\langle f_k | E_k \rangle|^2$, where $|f_k\rangle$ is the normalized perturbative approximation to the Floquet eigenstate and $|E_k\rangle$ is the eigenstate of \hat{H}_0 with the same index k in the perturbative expansion.

For non-degenerate perturbation theory, the normalized Floquet eigenstate is given by

$$|f_k\rangle = Z |f_k\rangle_u = Z \left(|E_k\rangle + \epsilon |f_k^{(1)}\rangle + \dots \right),$$

where Z is the normalization constant, $Z = \frac{1}{\sqrt{u \langle f_k | f_k \rangle_u}}$. Since $\langle E_k | f_k^{(i)} \rangle = 0$ for $i \geq 1$, the maximum overlap is given entirely by the squared normalization constant,

$$\mathcal{F}_{k,\max} = |\langle f_k | E_k \rangle|^2 = |Z|^2 = \frac{1}{u \langle f_k | f_k \rangle_u} = \frac{1}{1 + \langle f_k^{(1)} | f_k^{(1)} \rangle \epsilon^2 + 2\text{Re} [\langle f_k^{(1)} | f_k^{(2)} \rangle] \epsilon^3 + \dots}.$$

By expanding the previous equation in powers of ϵ , we obtain until fourth order

$$\begin{aligned} \mathcal{F}_{k,\max} &= 1 - a_2 \epsilon^2 - a_3 \epsilon^3 - a_4 \epsilon^4 - \dots \\ &= 1 - \langle f_k^{(1)} | f_k^{(1)} \rangle \epsilon^2 - 2\text{Re} [\langle f_k^{(1)} | f_k^{(2)} \rangle] \epsilon^3 - \left(2\text{Re} [\langle f_k^{(1)} | f_k^{(3)} \rangle] + \langle f_k^{(2)} | f_k^{(2)} \rangle - \langle f_k^{(1)} | f_k^{(1)} \rangle^2 \right) \epsilon^4 - \dots \end{aligned} \quad (\text{S.29})$$

The fact that $\mathcal{F}_{k,\max}$ does not contain terms of $\mathcal{O}(\epsilon^1)$ can be understood from the fact that $\langle E_k | f_k^{(1)} \rangle = 0$.

A. Second order term a_2

From the expression for $\langle E_{k'} | f_k^{(1)} \rangle$, Eq.(S.17), we obtain the second order correction

$$a_2 = \langle f_k^{(1)} | f_k^{(1)} \rangle = \sum_{k' \neq k} |\langle E_{k'} | f_k^{(1)} \rangle|^2 = \frac{1}{4} \sum_{k' \neq k} \frac{|\langle E_{k'} | \hat{K} | E_k \rangle|^2}{\sin^2 \left(\frac{\tau(E_{k'} - E_k)}{2} \right)}. \quad (\text{S.30})$$

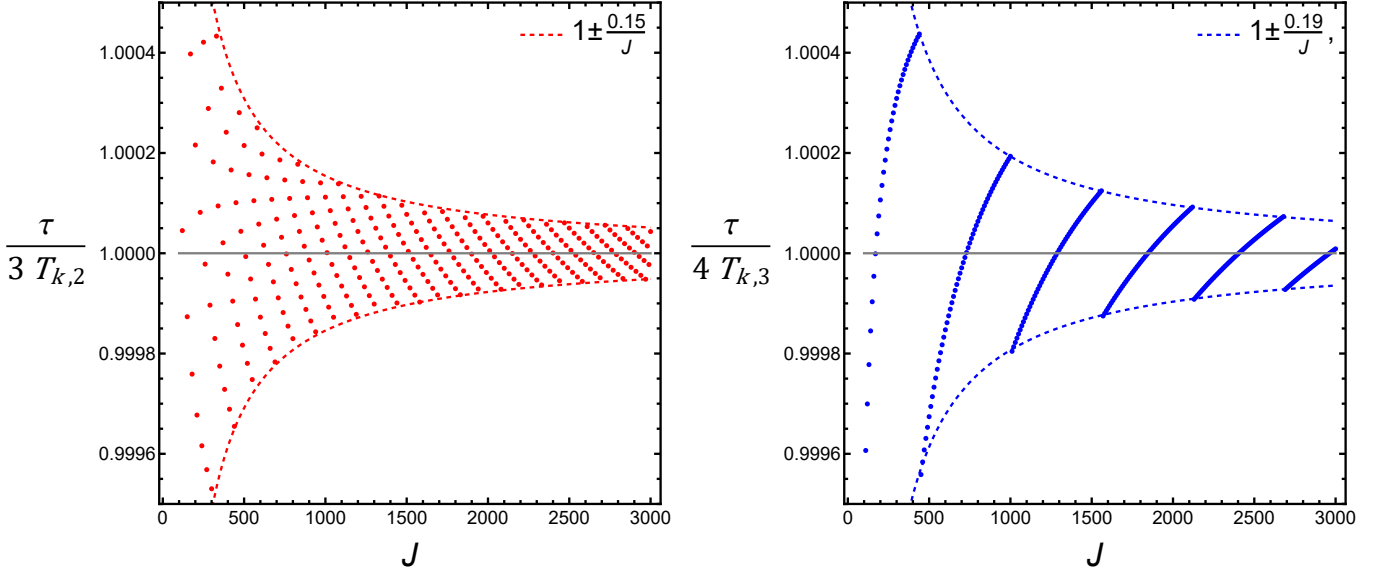


FIG. S.2. Ratio $\frac{\tau}{nT_{k,m}}$ that is closest to satisfying the resonant condition $\frac{\tau}{nT_{k,m}} = 1$ as a function of J for fixed kick period $\tau = 8$. Left panel is for resonance $m:n = 2:3$ and right panel for resonance $m:n = 3:4$. Dashed lines are fits to the decaying oscillations around 1 of the ratios $\frac{\tau}{nT_{k,m}}$.

The numerators in the terms of the previous sum depend on the squared norm of matrix elements of the kick operator. For kick operators with well defined classical limit, these matrix elements scale linearly with J for large enough J (see Fig. 3(e) in main text)

$$|\langle E_{k'} | \hat{K} | E_k \rangle| \approx C_{k',k} J.$$

As a consequence, the numerators give a_2 a quadratic dependence on J . If the state is non-resonant, the denominators evaluate to finite numbers, causing the whole term to scale quadratically with J , that is, $a_2 \propto J^2$ for non-resonant states.

However, if the state $|E_k\rangle$ is close to a resonance $m:n$, then for the term $k' = k+m$, we have $\tau(E_{k+m} - E_k)/2 = n\pi + \delta$, where δ approaches zero as $\delta = \delta_{m:n}/J$ (see Fig. 3(d) in main text and Fig. S.2). As a consequence, for this term $k' = k + m$, the denominator becomes small

$$\sin\left(\frac{\tau(E_{k+m} - E_k)}{2}\right) \approx \frac{\delta_{m:n}}{J},$$

and, consequently, the term with this small denominator in the sum in Eq.(S.30) acquire an additional J^2 scaling, leading to $a_2 \propto J^4$ for close-to-resonance states.

Similar small denominators appear in the terms of the sum when $k' = k + Mm$ for M integer and $M \geq 2$. For these terms we have

$$\sin\left(\frac{\tau(E_{k+Mm} - E_k)}{2}\right) \approx \sin\left(\frac{M\tau(E_{k+m} - E_k)}{2}\right) \approx \frac{M\delta_{m:n}}{J}.$$

The dependence on J of the square of these terms is shown in Figs. S.3(a) and S.4(a), for resonances $m:n = 1:1$ and $2:3$, respectively. Small denominators appear also for terms $k' = k - Mm$, for M integer and $M \geq 1$. In this case, $\sin\left(\frac{\tau(E_{k-Mm} - E_k)}{2}\right) \approx M\tilde{\delta}_{m:n}/J$, with $\tilde{\delta}_{m:n}$ slightly different from $\delta_{m:n}$. The square of these terms as a function of J is shown in Figs. S.3(b) and S.4(b), for resonances $m:n = 1:1$ and $2:3$, respectively. However, all the terms in the sum with these latter denominators are smaller than the one closest to the resonance, not only by the factor $1/M^2$ but also because, for the kick operator considered here, the matrix elements are smaller for more distant states $|\langle E_{k\pm Mm} | \hat{K} | E_k \rangle| < |\langle E_{k+m} | \hat{K} | E_k \rangle|$, see Fig. S.5. For resonances $m:n = 1:n$, the previous terms exhaust all the possible terms in the sum of Eq.(S.30) ($k' = k \pm 1M$), but for other resonances, $m \geq 2$, there are additional sum terms, that have no small denominators (see both panels of Fig. S.4). These remaining sum terms scale only quadratically with J .

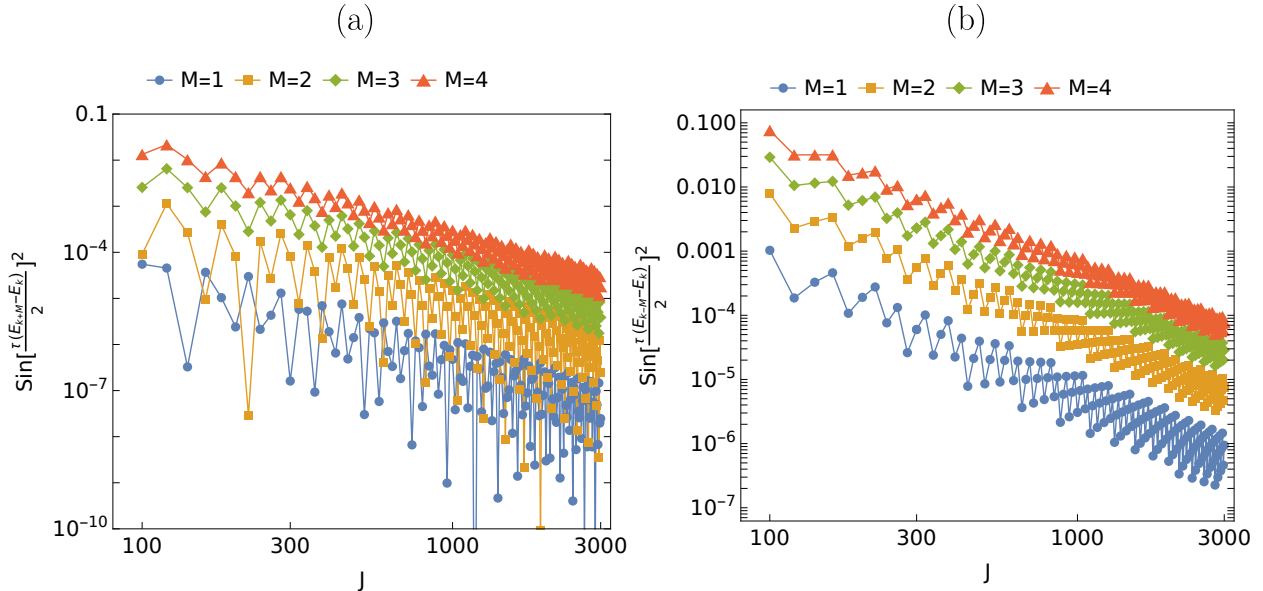


FIG. S.3. (a) Log-log plot of $\sin^2\left(\frac{\tau(E_{k+M}-E_k)}{2}\right)^2$ as a function of J for $M = 1, 2, 3$ and 4 for resonance $m:n = 1:1$, where E_k is the eigenvalue, for each J , that most closely satisfies the 1:1 resonant condition, $\tau(E_{k+1} - E_k)/2 = \pi$ for $\tau = 8$. (b) Similar to (a), but for $\sin^2\left(\frac{\tau(E_{k-M}-E_k)}{2}\right)^2$ vs J .

In summary, for states close to resonance, the coefficient a_2 has terms that scale as J^4 and other non-resonant terms that scale as J^2

$$a_2 = a_{2,\text{NR}} J^2 + a_{2,\text{CR}} J^4 \xrightarrow{J \rightarrow \infty} a_{2,\text{CR}} J^4,$$

where the quartic term dominates the quadratic one for large enough J (in the case of resonances with $m = 1$, the quadratic term is absent and the quartic term is dominant for all J). Meanwhile, for non-resonant states only the quadratic term is present

$$a_2 = a_{2,\text{NR}} J^2.$$

B. Third order term a_3

Similarly, for higher order corrections to $\mathcal{F}_{k,\text{max}}$ (Eq.(S.29)), we obtain the same splitting between non-resonant and close-to-resonant terms in the sum, where the latter ones appear only for states close to resonance. The scaling of J in the third order term is discussed in the following. From Eqs.(S.17) and (S.18), the term a_3 of the perturbative series for $\mathcal{F}_{k,\text{max}}$ can be written as

$$\begin{aligned} a_3 = 2\text{Re} \left[\langle f_k^{(1)} | f_k^{(2)} \rangle \right] &= \frac{1}{4} \sum_{k' \neq k} \sum_{k'' \neq k, k'} \frac{\cos\left(\frac{\tau(E_k - E_{k'})}{2}\right) \langle E_k | \hat{K} | E_{k'} \rangle \langle E_{k'} | \hat{K} | E_{k''} \rangle \langle E_{k''} | \hat{K} | E_k \rangle}{\sin\left(\frac{\tau(E_k - E_{k'})}{2}\right) \sin^2\left(\frac{\tau(E_k - E_{k'})}{2}\right)} \\ &+ \frac{1}{4} \sum_{k' \neq k} \frac{\cos\left(\frac{\tau(E_k - E_{k'})}{2}\right)}{\sin^3\left(\frac{\tau(E_k - E_{k'})}{2}\right)} \left| \langle E_k | \hat{K} | E_{k'} \rangle \right|^2 \left(\langle E_{k'} | \hat{K} | E_{k'} \rangle - \langle E_k | \hat{K} | E_k \rangle \right) \\ &+ \frac{1}{8} \sum_{k' \neq k} \frac{\langle E_k | \hat{K}^2 | E_{k'} \rangle \langle E_{k'} | \hat{K} | E_k \rangle - \langle E_k | \hat{K} | E_{k'} \rangle \langle E_{k'} | \hat{K}^2 | E_k \rangle}{\sin^2\left(\frac{\tau(E_k - E_{k'})}{2}\right)}. \end{aligned} \quad (\text{S.31})$$

In the second sum of the previous expression, we obtain a factor with the difference of diagonal matrix elements $\hat{K}_{k'k'} - \hat{K}_{kk}$. Each matrix element scales linearly with J but their difference tends to a constant for $J \rightarrow \infty$ (see

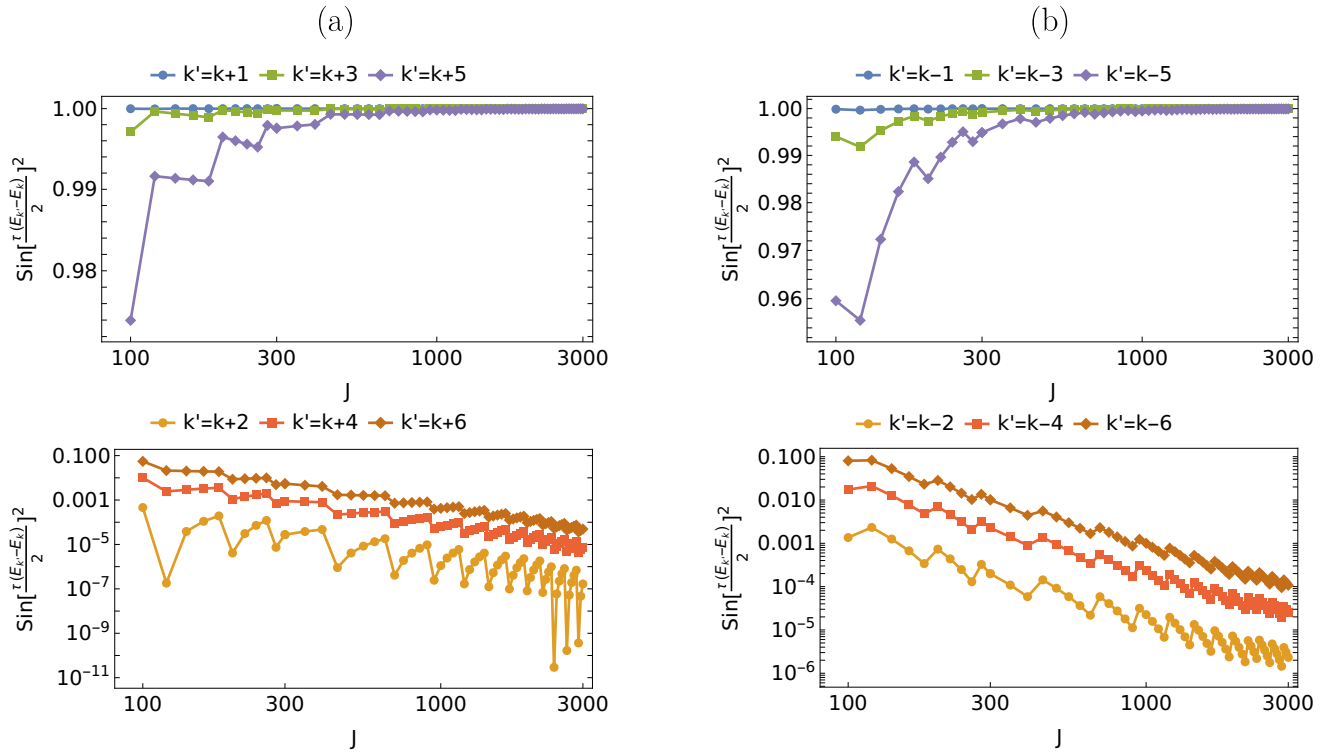


FIG. S.4. Log-log plots of $\sin^2\left(\frac{\tau(E_{k'} - E_k)}{2}\right)$ as a function of J for resonance $m:n = 2:3$, where E_k is the eigenvalue, for each J , that most closely satisfies the 2:3 resonant condition, $\tau(E_{k+2} - E_k)/2 = 3\pi$ for $\tau = 8$. In panel (a) $k' = k+1, k+3$ and $k+5$ are non-resonant terms and they are close 1 for all J , whereas $k' = k+2, k+4, k+6$ are close-to-resonance terms that go to zero as J increases. Panel (b) is the same for non-resonant ($k' = k-1, k-3$ and $k-5$) and close-to-resonance ($k' = k-2, k-4, k-6$) terms.

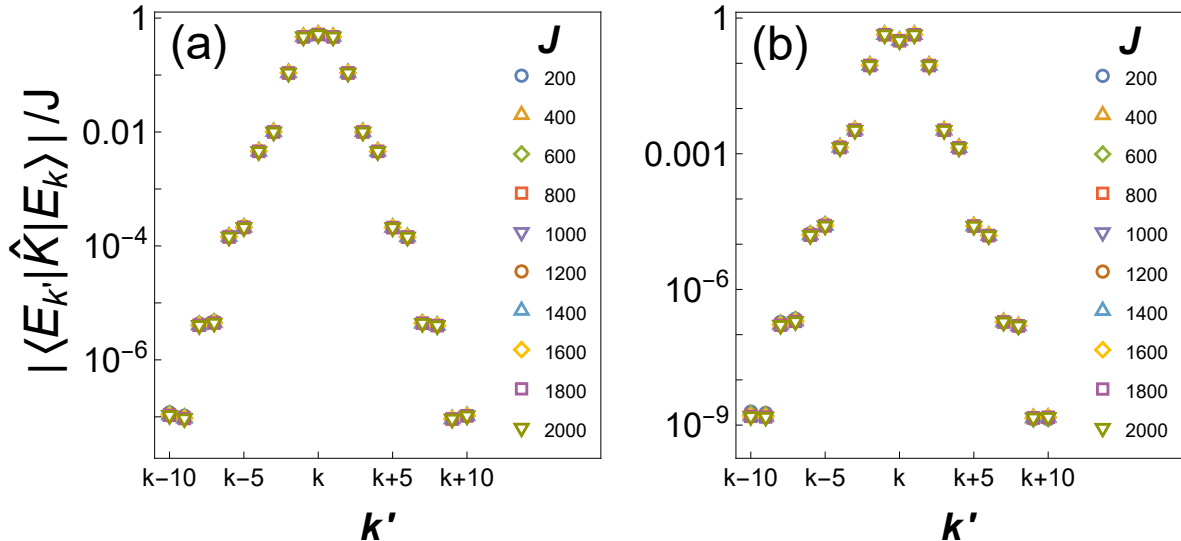


FIG. S.5. Log-linear plots of the magnitude of the kick-operator matrix elements divided by J , $|\langle E_{k'} | \hat{K} | E_k \rangle|/J$, where $|E_k\rangle$ is the \hat{H}_0 eigenstate that comes closest to satisfying the quantum resonant condition $m:n = 1:1$ [panel (a)] and $m:n = 2:3$ [panel (b)]. Diagonal and first ten neighbor states, $|E_{k'}\rangle$, above and below of $|E_k\rangle$ are plotted. Different values of J , indicated in the panels, were used.

Fig.S.10), therefore the numerators in the terms of this second sum scale only quadratically with J . Consequently, for non-resonant states this sum scales quadratically with J ; whereas for states close to a resonance, the sum contains non-resonant terms scaling quadratically and other close-to-resonant terms scaling as J^5 (where a factor of J^3 arises from small denominators). In the third sum, if the matrix elements of \hat{K} are real (as is the case considered in this work), the numerators vanish. The main contribution to a_3 in the limit $J \rightarrow \infty$ comes from the first sum, which scales as J^3 for non-resonant states, and as J^6 for close-to-resonance states (which includes terms scaling as J^3 and resonant terms with small denominators scaling as J^6). Thus,

$$a_3 = a_{3,\text{NR},1}J^2 + a_{3,\text{NR},2}J^3 \quad \text{for non-resonant states} \quad (\text{S.32})$$

$$a_3 = a_{3,\text{NR},1}J^2 + a_{3,\text{NR},2}J^3 + a_{3,\text{CR},1}J^5 + a_{3,\text{CR},2}J^6 \quad \text{for states close to resonance} \quad (\text{S.33})$$

In the limit $J \rightarrow \infty$, we obtain $a_3 \approx a_{3,\text{NR},2}J^3$ and $a_3 \approx a_{3,\text{CR},2}J^6$ for non-resonant and close-to-resonance states, respectively.

C. Scaling of ϵ_{max} from the perturbative series

A generalization of the dependence on J that we found for the second and third order perturbative coefficients of $\mathcal{F}_{k,\text{max}}$ explains the scaling obtained for ϵ_{max} in the main text, that is, $\epsilon_{\text{max}}^{\text{NR}} \propto 1/J$ and $\epsilon_{\text{max}}^{\text{CR}} \propto 1/J^2$. In previous subsection, we found that for large enough J , the coefficients for non-resonant states scale as $a_2 = a_{2,\text{NR}}J^2$ and $a_3 = a_{3,\text{NR}}J^3$, whereas for close-to-resonance states $a_2 = a_{2,\text{CR}}J^4$ and $a_3 = a_{3,\text{CR}}J^6$. The generalization of these scalings for higher-order coefficients, $a_p = a_{p,\text{NR}}J^p$ and $a_p = a_{p,\text{CR}}J^{2p}$, imply that the maximum fidelity is

$$\mathcal{F}_{k,\text{max}} = 1 - \sum_{p=2}^{p_o} a_p \epsilon^p = 1 - \sum_{p=2}^{p_o} a_{p,\text{NR}}(\epsilon J)^p$$

$$\mathcal{F}_{k,\text{max}} = 1 - \sum_{p=2}^{p_o} a_p \epsilon^p = 1 - \sum_{p=2}^{p_o} a_{p,\text{CR}}(\epsilon J^2)^p,$$

for resonant and close-to-resonance cases, respectively, where p_o is the order of the perturbative series that is needed to accurately describe $\mathcal{F}_{k,\text{max}}$ in the interval $\epsilon \in [0, \epsilon_{k,\text{max}}]$, where $\mathcal{F}_{k,\text{max}} \geq 1/2$. Regardless of p_o , we have that $\mathcal{F}_{k,\text{max}}$ is a function of variable $z = \epsilon J$ for non-resonant states and a function of variable $z = \epsilon J^2$ for states close to resonance. This differentiated dependence of $\mathcal{F}_{k,\text{max}}$ between resonant and close-to-resonance states allows us to explain the numerically observed scalings of ϵ_{max} , as explained in the main text and we discuss it in detail in the next paragraph.

In Fig. S.6(a), we show that the perturbative series of $\mathcal{F}_{k,\text{max}}$ up to $\mathcal{O}(\epsilon^2)$ becomes inaccurate well before $\mathcal{F}_{k,\text{max}}$ attains the value 1/2. In the figure, we compare the numerically exact and quadratic approximation of $\mathcal{F}_{k,\text{max}}$ as a function of ϵ , for $J = 500$ in the case of the state close to the resonance $m:n = 1:1$. The quadratic approximation accurately represents the numerical $\mathcal{F}_{k,\text{max}}$ only for a very small interval of ϵ close to zero. Higher order corrections are needed (at least up to order $p_o = 10$, yellow dashed-line in the same figure) to accurately describe the numerical results in the whole range $\epsilon \in [0, \epsilon_{k,\text{max}}]$. Even if the $\mathcal{O}(\epsilon^2)$ is unable to describe $\mathcal{F}_{k,\text{max}}$, our analysis and discussion about the perturbative series indicate that $\mathcal{F}_{k,\text{max}} = 1 - a_{2,\text{CR}}(\epsilon J)^2 - \dots - a_{10,\text{CR}}(\epsilon J)^{10}$. Then, to determine $\epsilon_{k,\text{max}}$ we have to find the roots of the degree-10 polynomial equation

$$1 - a_{2,\text{CR}}(\epsilon J^2)^2 - \dots - a_{10,\text{CR}}(\epsilon J^2)^{10} = 1 - a_{2,\text{CR}}z^2 - \dots - a_{10,\text{CR}}z^{10} = \frac{1}{2},$$

where $z = \epsilon J^2$. From the ten roots of the previous equation, one of them determines $\epsilon_{k,\text{max}}$. We call it z_{CR} . From this root, we have $\epsilon_{k,\text{max}} J^2 = z_{\text{CR}}$, i.e., $\epsilon_{k,\text{max}} = z_{\text{CR}}/J^2$, which is the scaling obtained numerically. Similarly, for non-resonant states, we solve a polynomial equation, but this time in terms of variable $z = \epsilon J$. If we call z_{NR} the relevant solution to the polynomial equation, we obtain $\epsilon_{k,\text{max}} = z_{\text{NR}}/J$, which is, again, the scaling obtained numerically.

Since the perturbative coefficients become very complicated for orders higher than $\mathcal{O}(\epsilon^3)$, it is a very hard task to verify from perturbative calculations that, for $p > 3$, $a_p = a_{2,\text{NR}}J^p$ and $a_p = a_{2,\text{CR}}J^{2p}$. However, it is possible to verify numerically that, indeed $\mathcal{F}_{k,\text{max}}$ is a function of $z = \epsilon J$ for non-resonant states and of $z = \epsilon J^2$ for close-to-resonance states in the interval of interest where $\mathcal{F}_{k,\text{max}} \geq 1/2$. This is done in Fig.S.7 for a non-resonant state. The figure shows $\mathcal{F}_{k,\text{max}}$ as a function of $z = \epsilon J$ for different values of J . It is clearly observed that all the curves cluster

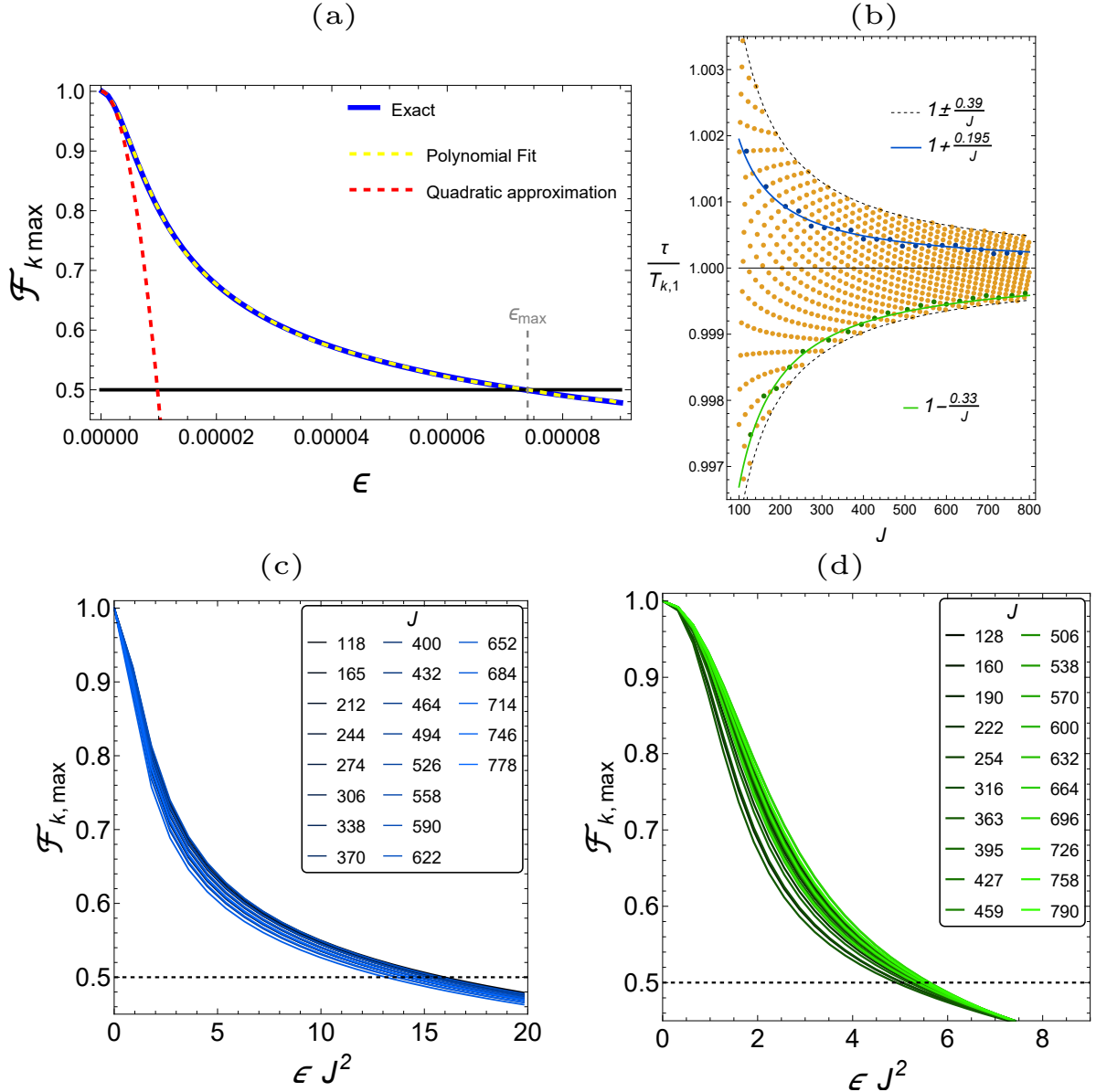


FIG. S.6. (a) Continuous blue line shows the exact numerical $\mathcal{F}_{k,\max}$ as a function of ϵ for the state closest to the resonance 1:1, for $\tau = 8$, and $J = 500$. Red dashed line is the perturbative approximation until second order in ϵ . The condition $\mathcal{F}_{k,\max} = 1/2$ (horizontal black line) determines ϵ_{\max} (vertical dashed line). Yellow dashed line is a polynomial of degree 10, $p(\epsilon) = 1 - \sum_{p=2}^{10} b_p \epsilon^p$, fitted to the exact numerical data. (b) Orange dots depict the kick period over the quantum period that is closest to satisfying the $m:n = 1:1$ quantum resonant condition $\frac{\tau}{T_{k,1}} = 1$ as a function of J . Coloured dots indicate values of J for which the ratio $\frac{\tau}{T_{k,1}}$ approaches 1 without oscillating, from above (blue dots) and from below (green dots). These values of J are used in panel (c) and (d), respectively. (c) $\mathcal{F}_{k,\max}$ as a function of $z = \epsilon J^2$ for the values of J corresponding to the blue dots of panel (b). (d) Same as panel (c) but for the green dots of panel (b).

around a common curve, which indicates that effectively, $F_{k,\max}$ is a function of $z = \epsilon J$. For close-to-resonance states a similar collapse of curves is obtained, however, in this case a more careful procedure has to be done to observe this. We already know that for states close to resonance, the ratio $\frac{\tau}{nT_{k,m}}$ oscillates around 1, with an amplitude that decays as $1/J$. To eliminate the effect of the oscillations, we select different values of J for which the ratio $\frac{\tau}{nT_{k,m}}$ decays without oscillating. In Fig. S.6(b), we indicate in blue and green two sets of J values for which the ratio $\frac{\tau}{T_{k,1}}$ (we consider the resonance $m:n = 1:1$) decays as $1/J$ without oscillating. One of these sets has ratios $\frac{\tau}{T_{k,1}} > 1$ (blue set) and the other has ratios $\frac{\tau}{T_{k,1}} < 1$ (green set). In panels (c) and (d) of Fig. S.6, we show the numerically

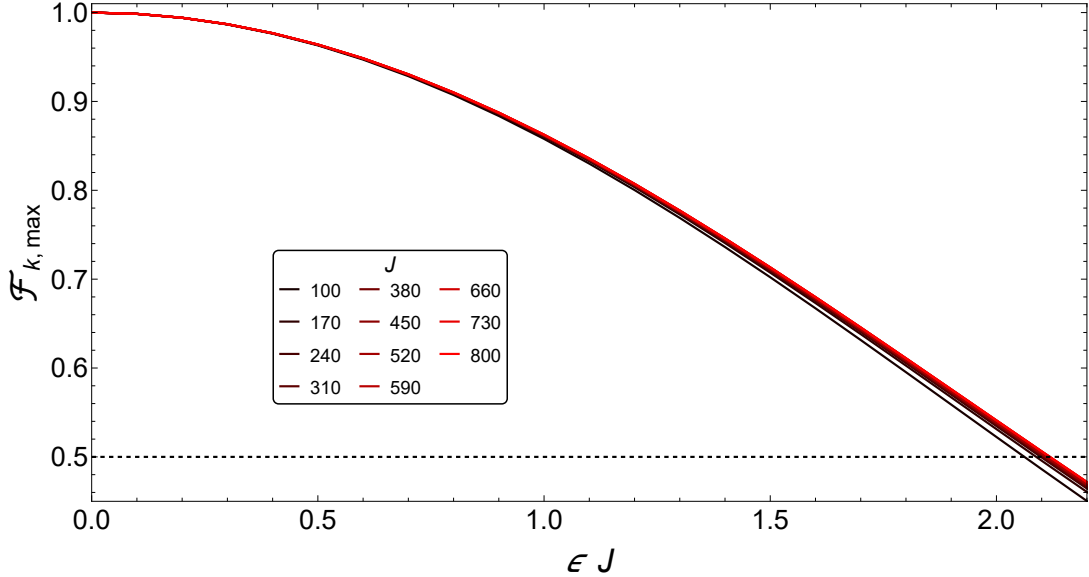


FIG. S.7. Numerically exact $\mathcal{F}_{k,\max}$ for a non-resonant state as a function of $z = \epsilon J$ for the indicated values of J . All the curves cluster around one common curve. For each value of J , we consider the state $|E_k\rangle$ with energy closest to $E_k \approx E/J = 0$, where no resonances are present.

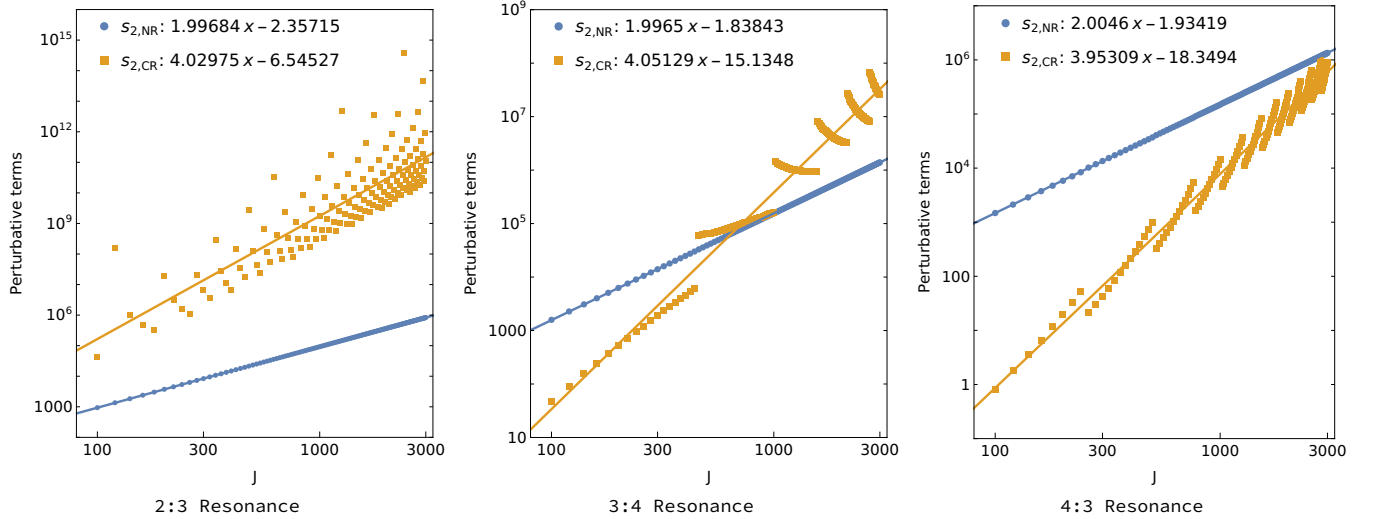


FIG. S.8. Log-log plots showing the close-to-resonant ($s_{2,CR}$, orange dots) and non-resonant ($s_{2,NR}$, blue dots) contributions to the second-order correction a_2 to $\mathcal{F}_{k,\max}$, as described in Eq. (S.34), as a function of J for the resonances 2:3, 3:4, and 4:3. Linear fits in ln-ln scale to the data points are indicated. Within the range shown, the close-to-resonant contribution $s_{2,CR}$ is dominant over the non-resonant contribution $s_{2,NR}$ only for the 2:3 resonance. From the fits shown in the panels: $s_{2,NR} \approx 0.09469 J^2$ and $s_{2,CR} \approx 0.001437 J^4$ for resonance 2:3; $s_{2,NR} \approx 0.1591 J^2$ and $s_{2,CR} \approx 2.673 \times 10^{-7} J^4$ for resonance 3:4; and $s_{2,NR} \approx 0.1445 J^2$ and $s_{2,CR} \approx 1.074 \times 10^{-8} J^4$ for resonance 4:3.

exact evaluation of $\mathcal{F}_{k,\max}$ as a function of $z = \epsilon J^2$, for all the values of J in each set. We observe that, indeed, all the curves cluster around the same common curve, substantiating our claim that $\mathcal{F}_{k,\max}$ is a function of $z = \epsilon J^2$ for close-to-resonance states.

D. Dominance of the largest power of J in the coefficients of the $\mathcal{F}_{k,\max}$ perturbative series

In order to obtain the universal scalings of ϵ_{\max} in the limit $J \rightarrow \infty$, it is necessary for the terms with the largest power of J in the coefficients of the perturbative series of $\mathcal{F}_{k,\max}$ to dominate. Here, we analyze how large J must be

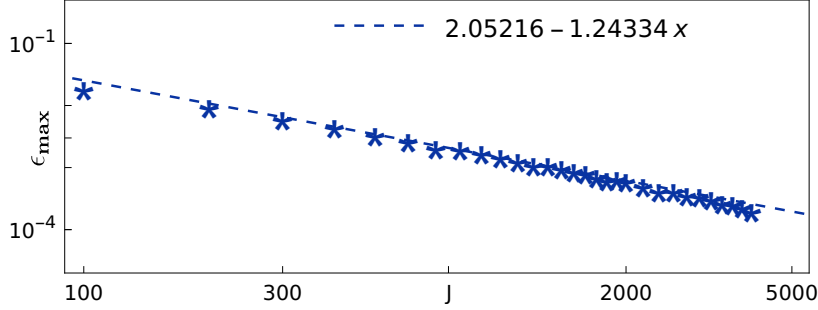


FIG. S.9. Log-log plot showing the scaling of $\epsilon_{\max}^{\text{CR}}$ with J for 3:4 resonance. For the range of J values considered, we get $\epsilon_{\max}^{\text{CR}} \propto J^{-1.24}$, far from J^{-2} . As explained in subsection IV D, $J > 2.4 \times 10^4$ needs to be considered to obtain a scaling of J^{-2} . Data available at [53] in the main text.

for this condition to be met in the close-to-resonance case, and discuss whether the numerically available values of J are large enough for the resonances 1:1, 2:3 and 3:4 in the case of the Hamiltonian we consider in the main text.

As an example, we consider the close to $m:n = 2:3$ resonance case. First, we split the sum in Eq.(S.30) as

$$a_2 = s_{2,\text{CR}} + s_{2,\text{NR}}, \quad (\text{S.34})$$

where $s_{2,\text{CR}}$ contains close-to-resonance terms and $s_{2,\text{NR}}$ contains the remaining ones. The close-to-resonance terms are those that approximately satisfy $\tau(E_{k'} - E_k)/2 \approx 3\pi$, i.e., those with $k' = k \pm 2M$ where M is a strictly-positive integer. These terms give

$$s_{2,\text{CR}} = \frac{1}{4} \sum_{M=\pm 1, \pm 2, \dots} \frac{|\langle E_{k+2M} | \hat{K} | E_k \rangle|^2}{\sin^2 \left(\frac{\tau(E_{k+2M} - E_k)}{2} \right)}.$$

From all these terms, the most important is the one closest to the resonant condition, $M = 1$. Thus,

$$s_{2,\text{CR}} \approx \frac{|\langle E_{k+2} | \hat{K} | E_k \rangle|^2}{4 \sin^2 \left(\frac{\tau(E_{k+2} - E_k)}{2} \right)} \approx \frac{|\langle E_{k+2} | \hat{K} | E_k \rangle|^2 J^2}{4 \delta_{2:3}^2} \approx \frac{C_{k+2,k}^2}{4 \delta_{2:3}^2} J^4 = a_{2,\text{CR}} J^4,$$

where we have used that $\tau(E_{k+2} - E_k)/2 \approx 3\pi + \delta_{2:3}/J$, and expressed $|\langle E_{k+2} | \hat{K} | E_k \rangle| = C_{k+2,k} J$.

From all the remaining (non-resonant) terms, the most important are the ones involving first neighbors ($k' = k \pm 1$)

$$s_{2,\text{NR}} \approx \frac{|\langle E_{k+1} | \hat{K} | E_k \rangle|^2}{4 \sin^2 \left(\frac{\tau(E_{k+1} - E_k)}{2} \right)} + \frac{|\langle E_{k-1} | \hat{K} | E_k \rangle|^2}{4 \sin^2 \left(\frac{\tau(E_{k-1} - E_k)}{2} \right)} \approx$$

$$\frac{|\langle E_{k+1} | \hat{K} | E_k \rangle|^2}{4} + \frac{|\langle E_{k-1} | \hat{K} | E_k \rangle|^2}{4} \approx \frac{|\langle E_{k+1} | \hat{K} | E_k \rangle|^2}{2} \approx \frac{C_{k+1,k}^2}{2} J^2 = a_{2,\text{NR}} J^2,$$

where we have used $\tau(E_{k\pm 1} - E_k)/2 \approx \tau(E_{k\pm 2} - E_k)/4 \approx \pm 3\pi/2$ [using aforementioned condition for 2:3 resonance and $E_{k\pm 2} - E_k \approx 2(E_{k\pm 1} - E_k)$], assumed that $|\langle E_{k+1} | \hat{K} | E_k \rangle| \approx |\langle E_{k-1} | \hat{K} | E_k \rangle|$, and expressed $|\langle E_{k+1} | \hat{K} | E_k \rangle| = C_{k+1,k} J$. From the previous expressions, the condition of dominance of the quartic term, $a_{2,\text{NR}} J^2 \ll a_{2,\text{CR}} J^4$, can be written as

$$\frac{2|\delta_{2:3}|C_{k+1,k}}{C_{k+2,k}} \ll J.$$

For the case studied in the main text, and using a tolerance of 10^{-3} for the ratio between non-resonant and resonant terms ($a_{2,\text{NR}} J^2 = 10^{-3} a_{2,\text{CR}} J^4$, see numerical estimates of $a_{2,\text{NR}}$ and $a_{2,\text{CR}}$ in Fig. S.8), we obtain $J > 256$ for resonance 2:3, which are available system sizes for our numerical methods.

Repetition of the same analysis for resonance 3:4 results in the condition

$$\frac{2|\delta_{3:4}|C_{k+1,k}}{C_{k+3,k}} \ll J,$$

where $|\langle E_{k+3} | \hat{K} | E_k \rangle| \approx C_{k+3,k} J$, and $\tau(E_{k+3} - E_k)/2 \approx 4\pi + \delta_{3:4}/J$. Considering the same tolerance as before ($a_{2,\text{NR}} J^2 = 10^{-3} a_{2,\text{CR}} J^4$, see Fig. S.8 for numerical estimations of $a_{2,\text{NR}}$ and $a_{2,\text{CR}}$), we now obtain $J > 24393$, which is beyond the values of J we consider in this work. As a consequence, the dominant scaling of ϵ_{max} for $J \rightarrow \infty$ is achieved for moderate system sizes for low-order resonances 1:1 and 2:3, while for higher-order resonances (3:4 and others), we would have to consider larger values of J . This is illustrated in Fig. S.8, where the close-to-resonant $s_{2,\text{CR}}$ and non-resonant $s_{2,\text{NR}}$ parts of a_2 are plotted as a function of J in the range $J \in [100, 3000]$ for three resonances: 2:3, 3:4 and 4:3. In the case of resonance 2:3, the close-to-resonance part $s_{2,\text{CR}}$ is much larger than $s_{2,\text{NR}}$, while for the other resonances the close-to-resonant part $s_{2,\text{CR}}$ is barely larger or even smaller than the non-resonant part $s_{2,\text{NR}}$. From this, it is concluded that the universal scaling for ϵ_{max} is available for moderate sizes of $J \in [100, 4000]$ in the case of resonance 1:1 (for this resonance, the non-resonant contribution vanishes, $s_{2,\text{NR}} = 0$) and resonance 2:3. For the resonance 3:4, much larger values of J than those used in this work are needed, such as $J \in [24000, 2.4 \times 10^5]$. In Fig. S.9, we show the ϵ_{max} scaling analysis for this resonance $m:n = 3:4$ in the range $J \in [100, 4000]$, similar to those shown in Fig. 3(b) of the main text for resonances $m:n = 1:1$ and 2:3. Unlike those resonances, in this case we obtain $\epsilon_{\text{max}} \propto J^{1.243}$, very far from the expected scaling for $J \rightarrow \infty$, $\epsilon_{\text{max}} \propto J^2$.

V. PERTURBATIVE SERIES FOR \mathcal{F}_{max} : EXACT RESONANCE CASE

In this section, we present the details to obtain perturbatively \mathcal{F}_{max} in the case of an exact resonance involving states $|E_k\rangle$ and $|E_{k+m}\rangle$. We analyze the dependence on J of its different terms and from that we analytically obtain the scaling of ϵ_{max} with the system size, J .

The normalized Floquet eigenstate in degenerate perturbation theory, which applies for exact resonant states, is

$$|f_a\rangle = \frac{1}{\sqrt{1 + \epsilon^2 \langle f_a^{(1)} | f_a^{(1)} \rangle + \mathcal{O}(\epsilon^3)}} \left(|f_a^{(0)}\rangle + \epsilon |f_a^{(1)}\rangle + \epsilon^2 |f_a^{(2)}\rangle + \mathcal{O}(\epsilon^3) \right) = \quad (\text{S.35})$$

$$\left(1 - \frac{1}{2} \langle f_a^{(1)} | f_a^{(1)} \rangle \epsilon^2 \right) |f_a^{(0)}\rangle + \epsilon |f_a^{(1)}\rangle + \epsilon^2 |f_a^{(2)}\rangle + \mathcal{O}(\epsilon^3). \quad (\text{S.36})$$

From this, the maximum overlap of the Floquet eigenstate is obtained by consistently expanding in powers of ϵ the squared norm $|\langle E_a | f_a \rangle|^2$. The result up to $\mathcal{O}(\epsilon^2)$ is

$$\mathcal{F}_{a,\text{max}} = |\langle E_a | f_a \rangle|^2 = \left(1 - \epsilon^2 \langle f_a^{(1)} | f_a^{(1)} \rangle \right) |\langle E_a | f_a^{(0)} \rangle|^2 + 2\text{Re} \left[\langle E_a | f_a^{(0)} \rangle \langle E_a | f_a^{(1)} \rangle^* \right] \epsilon + \quad (\text{S.37})$$

$$\begin{aligned} & \left(|\langle E_a | f_a^{(1)} \rangle|^2 + 2\text{Re} \left[\langle E_a | f_a^{(0)} \rangle \langle E_a | f_a^{(2)} \rangle^* \right] \right) \epsilon^2 = \\ & \left(1 - \epsilon^2 \sum_{k' \neq a, a'} |\langle E_{k'} | f_a^{(1)} \rangle|^2 \right) |\langle E_a | f_a^{(0)} \rangle|^2 + 2\text{Re} \left[\langle E_a | f_a^{(0)} \rangle \langle f_{a'}^{(0)} | E_a \rangle \langle f_a^{(1)} | f_{a'}^{(0)} \rangle \right] \epsilon + \\ & \left[|\langle E_a | f_{a'}^{(0)} \rangle|^2 - |\langle E_a | f_a^{(0)} \rangle|^2 \right] |\langle f_{a'}^{(0)} | f_a^{(1)} \rangle|^2 \epsilon^2 + 2\text{Re} \left[\langle E_a | f_a^{(0)} \rangle \langle E_a | f_a^{(2)} \rangle^* \right] \epsilon^2, \end{aligned} \quad (\text{S.38})$$

where $a, a' = k$ or $k + m$ ($a' \neq a$) and in the last equality we have used $\langle E_a | f_a^{(1)} \rangle = \langle E_a | f_{a'}^{(0)} \rangle \langle f_{a'}^{(0)} | f_a^{(1)} \rangle$ and

$$\langle f_a^{(1)} | f_a^{(1)} \rangle = \sum_{k' \neq a, a'} |\langle E_{k'} | f_a^{(1)} \rangle|^2 + |\langle f_{a'}^{(0)} | f_a^{(1)} \rangle|^2.$$

We will show that the maximal fidelity for large J can be very well approximated by considering only the first term of Eq. (S.38),

$$\mathcal{F}_{a,\text{max}} = |\langle E_a | f_a \rangle|^2 \approx \left(1 - \epsilon^2 \sum_{k' \neq a, a'} |\langle E_{k'} | f_a^{(1)} \rangle|^2 \right) |\langle E_a | f_a^{(0)} \rangle|^2. \quad (\text{S.39})$$

In order to show this, we now determine the dependence on J of the different terms in the complete expression of $\mathcal{F}_{a,\text{max}}$, Eq. (S.38). We begin by analyzing the dependence on J of the sum in the first term of Eq. (S.38),

$$\sum_{k' \neq a, a'} |\langle E_{k'} | f_a^{(1)} \rangle|^2 = \sum_{k' \neq a, a'} \frac{|\langle E_{k'} | \hat{K} | f_a^{(0)} \rangle|^2}{4 \sin^2 \left(\frac{\tau(E_{k'} - E_a)}{2} \right)}.$$

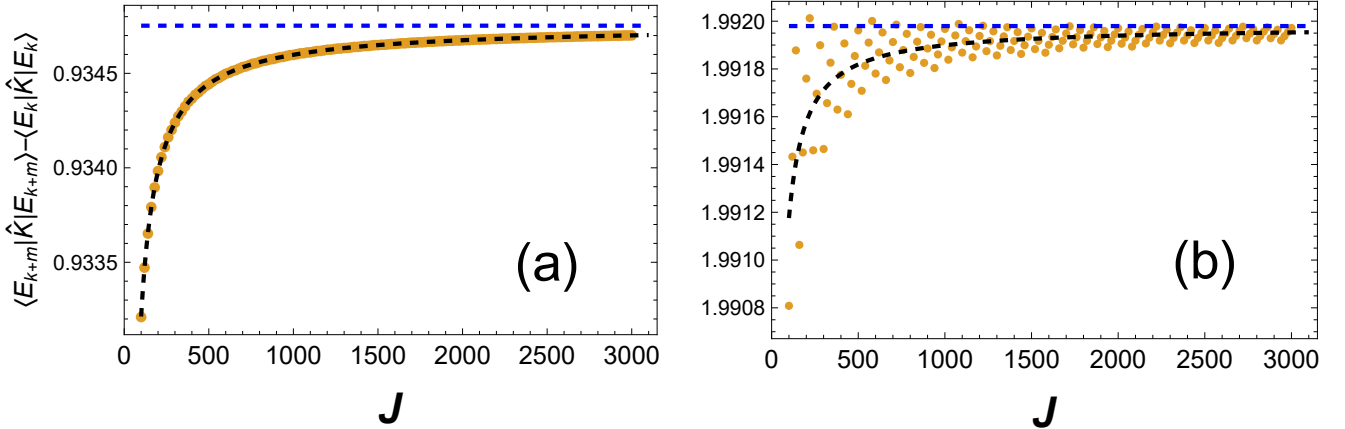


FIG. S.10. Orange dots depict $(\langle E_{k+m} | \hat{K} | E_{k+m} \rangle - \langle E_k | \hat{K} | E_k \rangle)$ vs J , where $|E_k\rangle$ is the \hat{H}_0 eigenstate that comes closest to satisfying the quantum resonant condition $m:n$. Panel (a) is for resonance $m:n = 1:1$ and (b) for resonance $m:n = 2:3$. It can be observed that these differences, for large J , tend to a constant value, κ_o (blue dashed lines). Black dashed lines are fits of the form $\kappa_o + \frac{C}{J}$.

Similar to states close to resonance, this sum scales as J^4 . This scaling comes from the linear scaling of the matrix elements and from small denominators. In order to simplify the presentation, from now on, we assume that $a = k$ and $a' = k + m$. The dominant terms with small denominators in the sum are those coming from $k' = a - m$ and $k' = a + 2m$, for which $\tau(E_{k+2m} - E_k) \approx 4\pi n + \frac{\delta_{m:n}}{J}$ and $\tau(E_{k-m} - E_k) \approx -2\pi n + \frac{\delta_{m:n}}{J}$. From this, we obtain

$$\sum_{k' \neq a, a'} \frac{|\langle E_{k'} | \hat{K} | f_a^{(0)} \rangle|^2}{4 \sin^2 \left(\frac{\tau(E_{k'} - E_a)}{2} \right)} \approx \frac{|\langle E_{k-m} | \hat{K} | f_k^{(0)} \rangle|^2}{4\delta_{m:n}^2} J^2 + \frac{|\langle E_{k+2m} | \hat{K} | f_k^{(0)} \rangle|^2}{4\delta_{m:n}^2} J^2 = D_o J^4. \quad (\text{S.40})$$

A. Dependence on J of $\langle E_a | f_a^{(0)} \rangle$ and $\langle E_a | f_{a'}^{(0)} \rangle$

Now we analyze the dependence on J of $\langle E_a | f_a^{(0)} \rangle$ and $\langle E_a | f_{a'}^{(0)} \rangle$. To do that, we have to diagonalize the kick operator in the degenerate subspace, Eq. (S.25). The scaling of its matrix elements is linear

$$K_{k+m,k} = \langle E_{k+m} | \hat{K} | E_k \rangle = \kappa J \quad (\text{S.41})$$

$$K_{k,k} = \langle E_k | \hat{K} | E_k \rangle = \kappa_1 J \quad (\text{S.42})$$

$$K_{k+m,k+m} = \langle E_{k+m} | \hat{K} | E_{k+m} \rangle = \kappa_2 J, \quad (\text{S.43})$$

where we have assumed that the non-diagonal term $K_{k+m,k}$ is real and without loss of generality $K_{k+m,k} > 0$, which implies that $\kappa > 0$. The diagonal matrix elements scale linearly with J but, as shown in Figure S.10, their difference tends to be constant in the limit $J \rightarrow \infty$,

$$\lim_{J \rightarrow \infty} (\langle E_{k+m} | \hat{K} | E_{k+m} \rangle - \langle E_k | \hat{K} | E_k \rangle) = \kappa_o.$$

From the previous behavior of the matrix elements, the matrix to be diagonalized for large J is

$$\begin{pmatrix} K_{k,k} & K_{k,k+m} \\ K_{k+m,k} & K_{k+m,k+m} \end{pmatrix} = K_{k,k} \begin{pmatrix} 1 & 0 \\ 0 & 1 \end{pmatrix} + \begin{pmatrix} 0 & K_{k,k+m} \\ K_{k+m,k} & K_{k+m,k+m} - K_{k,k} \end{pmatrix} \xrightarrow{J \rightarrow \infty} \kappa_1 J \begin{pmatrix} 1 & 0 \\ 0 & 1 \end{pmatrix} + J \begin{pmatrix} 0 & \kappa \\ \kappa & \kappa_o/J \end{pmatrix}. \quad (\text{S.44})$$

The eigenvalues and eigenvectors of this matrix, at leading order in $1/J$, are

$$\phi_k^{(1)} = (\kappa_1 - \kappa)J + \frac{\kappa_o}{2} + \mathcal{O}\left(\frac{1}{J}\right) \quad (\text{S.45})$$

$$\phi_{k+m}^{(1)} = (\kappa_1 + \kappa)J + \frac{\kappa_o}{2} + \mathcal{O}\left(\frac{1}{J}\right) \quad (\text{S.46})$$

and

$$|f_k^{(0)}\rangle = \frac{1}{\sqrt{2}} \left(1 + \frac{\kappa_o}{4\kappa J}\right) |E_k\rangle - \frac{1}{\sqrt{2}} \left(1 - \frac{\kappa_o}{4\kappa J}\right) |E_{k+m}\rangle + \mathcal{O}\left(\frac{1}{J^2}\right) \quad (\text{S.47})$$

$$|f_{k+m}^{(0)}\rangle = \frac{1}{\sqrt{2}} \left(1 - \frac{\kappa_o}{4\kappa J}\right) |E_k\rangle + \frac{1}{\sqrt{2}} \left(1 + \frac{\kappa_o}{4\kappa J}\right) |E_{k+m}\rangle + \mathcal{O}\left(\frac{1}{J^2}\right), \quad (\text{S.48})$$

where, in order to label the states $|f_a^{(0)}\rangle$ and $\phi_a^{(1)}$ we have assumed that $\kappa_0 > 0$ (if $\kappa_0 < 0$ the labels simply have to be interchanged). From the previous equations we obtain

$$c_{k,1} = \langle E_k | f_k^{(0)} \rangle = \frac{1}{\sqrt{2}} \left(1 + \frac{\kappa_o}{4\kappa J}\right) + \mathcal{O}\left(\frac{1}{J^2}\right) \quad (\text{S.49})$$

$$c_{k+m,1} = \langle E_k | f_{k+m}^{(0)} \rangle = \frac{1}{\sqrt{2}} \left(1 - \frac{\kappa_o}{4\kappa J}\right) + \mathcal{O}\left(\frac{1}{J^2}\right). \quad (\text{S.50})$$

and

$$|\langle E_k | f_k^{(0)} \rangle|^2 = \frac{1}{2} + \frac{\kappa_o}{4\kappa J} + \mathcal{O}\left(\frac{1}{J^2}\right) \quad (\text{S.51})$$

$$|\langle E_k | f_{k+m}^{(0)} \rangle|^2 = \frac{1}{2} - \frac{\kappa_o}{4\kappa J} + \mathcal{O}\left(\frac{1}{J^2}\right). \quad (\text{S.52})$$

B. Dependence on J of $\langle f_{a'}^{(0)} | f_a^{(1)} \rangle$

The second and third terms in Eq. (S.38) depend on $\langle f_{a'}^{(0)} | f_a^{(1)} \rangle$ given in Eq.(S.28). For $a = k$ and $a' = k + m$ this overlap is

$$\langle f_{k+m}^{(0)} | f_k^{(1)} \rangle = -\frac{i}{\phi_k^{(1)} - \phi_{k+m}^{(1)}} \left(\sum_{k' \neq k, k+m} \frac{\langle f_{k+m}^{(0)} | \hat{K} | E_{k'} \rangle \langle E_{k'} | \hat{K} | f_k^{(0)} \rangle}{e^{i\tau(E_{k'} - E_k)} - 1} + \frac{1}{2} \langle f_{k+m}^{(0)} | \hat{K}^2 | f_k^{(0)} \rangle \right). \quad (\text{S.53})$$

The first expression inside the parentheses of the previous equation is a sum that, again, is dominated by the terms with small denominators. Among those terms, the largest ones, for an exact resonance $m:n$, are those with $k' = k - m$ and $k' = k + 2m$. For these terms, $\tau(E_{k-m} - E_k) = -2\pi n + 2\delta_{m:n}/J$ and $\tau(E_{k+2m} - E_k) = 4\pi n + 2\delta_{m:n}/J$, which imply $e^{i\tau(E_{k-m} - E_k)} \approx e^{i\tau(E_{k+2m} - E_k)} \approx e^{2i\delta_{m:n}/J} \approx 1 + 2i\delta_{m:n}/J$. Therefore, the sum is approximated as

$$\sum_{k' \neq k, k+m} \frac{\langle f_{k+m}^{(0)} | \hat{K} | E_{k'} \rangle \langle E_{k'} | \hat{K} | f_k^{(0)} \rangle}{e^{i\tau(E_{k'} - E_k)} - 1} \approx \frac{\langle f_{k+m}^{(0)} | \hat{K} | E_{k-m} \rangle \langle E_{k-m} | \hat{K} | f_k^{(0)} \rangle}{2i\delta_{m:n}} J + \frac{\langle f_{k+m}^{(0)} | \hat{K} | E_{k+2m} \rangle \langle E_{k+2m} | \hat{K} | f_k^{(0)} \rangle}{2i\delta_{m:n}} J. \quad (\text{S.54})$$

Now, by using the zero order approximations to the Floquet eigenstates, Eqs.(S.47) and (S.48), we obtain that the products in the numerators of the previous expression are

$$\langle f_{k+m}^{(0)} | \hat{K} | E_{k'} \rangle \langle E_{k'} | \hat{K} | f_k^{(0)} \rangle \approx \frac{1}{2} \left[|\langle E_k | \hat{K} | E_{k'} \rangle|^2 - |\langle E_{k+m} | \hat{K} | E_{k'} \rangle|^2 \right].$$

Substituting this expression in (S.54), we obtain

$$\sum_{k' \neq k, k+m} \frac{\langle f_{k+m}^{(0)} | \hat{K} | E_{k'} \rangle \langle E_{k'} | \hat{K} | f_k^{(0)} \rangle}{e^{i\tau(E_{k'} - E_k)} - 1} \approx \frac{|\langle E_k | \hat{K} | E_{k-m} \rangle|^2 - |\langle E_{k+m} | \hat{K} | E_{k-m} \rangle|^2}{4i\delta_{m:n}} J +$$

$$\frac{|\langle E_k | \hat{K} | E_{k+2m} \rangle|^2 - |\langle E_{k+m} | \hat{K} | E_{k+2m} \rangle|^2}{4i\delta_{m:n}} J \approx \frac{|\langle E_k | \hat{K} | E_{k-m} \rangle|^2 - |\langle E_{k+m} | \hat{K} | E_{k+2m} \rangle|^2}{4i\delta_{m:n}} J,$$

where in the last step we have neglected matrix elements between states with an index distance of $2m$ and kept only those with an index distance of m , $|\langle E_k | \hat{K} | E_{k-m} \rangle| \gg |\langle E_{k+m} | \hat{K} | E_{k-m} \rangle|$ and $|\langle E_{k+m} | \hat{K} | E_{k+2m} \rangle| \gg |\langle E_k | \hat{K} | E_{k+2m} \rangle|$. The numerator in the resulting expression depends on two matrix elements of the same order that scale quadratically with J , but their difference scales only linearly. Therefore, by considering the factor J coming from the small denominator, we get that the whole sum scales only quadratically with J , that is

$$\sum_{k' \neq k, k+m} \frac{\langle f_{a'}^{(0)} | \hat{K} | E_{k'} \rangle \langle E_{k'} | \hat{K} | f_a^{(0)} \rangle}{e^{i\tau(E_{k'} - E_a)} - 1} = -iB_1 J^2.$$

Now, we focus on the second expression between the parentheses of Eq. (S.53)

$$\langle f_{k+m}^{(0)} | \hat{K}^2 | f_k^{(0)} \rangle = \frac{1}{2} \left[\langle E_k | \hat{K}^2 | E_k \rangle - \langle E_{k+m} | \hat{K}^2 | E_{k+m} \rangle + \frac{\kappa_o}{J} \langle E_k | \hat{K}^2 | E_{k+m} \rangle \right]$$

where we have used the zero order Floquet eigenstates at leading order in $1/J$, Eqs.(S.47) and (S.48), and assumed that $\langle E_k | \hat{K}^2 | E_{k+m} \rangle$ is real. The resulting expression depends on the difference of diagonal matrix elements of \hat{K}^2 . Every matrix element scales quadratically with J , but their difference does it only linearly. The last term is divided by J , then it only scales linearly with J . Consequently, the whole term scales linearly with J

$$\langle f_{a'}^{(0)} | \hat{K}^2 | f_a^{(0)} \rangle = \frac{1}{2} \left[\langle E_a | \hat{K}^2 | E_a \rangle - \langle E_{a'} | \hat{K}^2 | E_{a'} \rangle + \frac{\kappa_o}{J} \langle E_a | \hat{K}^2 | E_{a'} \rangle \right] = B_o J.$$

Now, according to Eqs.(S.45) and (S.46), the difference of first order corrections to the quasienergies is

$$\phi_k^{(1)} - \phi_{k+m}^{(1)} \approx -2\kappa J.$$

Putting all these results together, we conclude that

$$\langle f_{a'}^{(0)} | f_a^{(1)} \rangle \approx \frac{B_1}{2\kappa} J + i \frac{B_o}{4\kappa}. \quad (\text{S.55})$$

Based on this scaling behavior of $\langle f_{a'}^{(0)} | f_a^{(1)} \rangle$, the terms containing this inner product in Eq.(S.38) can be shown to be negligible with respect to the first term in the same equation. This justifies the validity of Eq.(S.39), as discussed in the following subsection.

C. Scaling of ϵ_{\max} for exact resonances

By substituting the results of the previous subsections [Eqs. (S.40),(S.49)-(S.52) (S.55)] in Eq.(S.38), we conclude that, for large enough J , the dependence on J of the maximum fidelity is

$$\mathcal{F}_{k,\max} = (1 - D_o J^4 \epsilon^2) \left(\frac{1}{2} + \frac{\kappa_o}{4\kappa J} \right) + \frac{B_1}{2\kappa} J \epsilon - \frac{\kappa_o}{2\kappa} \left[\left(\frac{B_1^2}{4\kappa^4} \right) J + \frac{B_o^2}{16\kappa^2 J} \right] \epsilon^2 + T_2 \epsilon^2,$$

where $T_2 = 2\text{Re}[\langle E_a | f_a^{(0)} \rangle \langle E_a | f_a^{(2)} \rangle^*]$ remains to be determined. First and third terms are both quadratic in ϵ , but, since the third term scales linearly with J and the first one scales as J^4 , the third term is clearly negligible compared to the first term for large J . On the other hand, the second term depends on the combination $z = J\epsilon$, whereas the first one depends on $J^4 \epsilon^2 = z^2 J^2$. Therefore, for large enough J , the first term dominates over the second one. We conclude that

$$\mathcal{F}_{k,\max} = (1 - D_o J^4 \epsilon^2) \left(\frac{1}{2} + \frac{\kappa_o}{4\kappa J} \right) + T_2 \epsilon^2. \quad (\text{S.56})$$

The coefficient T_2 requires calculating the second order correction to the Floquet eigenstates in degenerate perturbation theory, a direct but cumbersome task. Instead of that, we evaluate numerically the relevance of this term by plotting the exact numerical evaluation of $\mathcal{F}_{k,\max}$ and compare it with the result obtained from the first term in Eq.(S.56). This is done in Fig. S.11 for an exact resonance 1:1 with $J = 1000$. We see that the exact numerical evaluation of

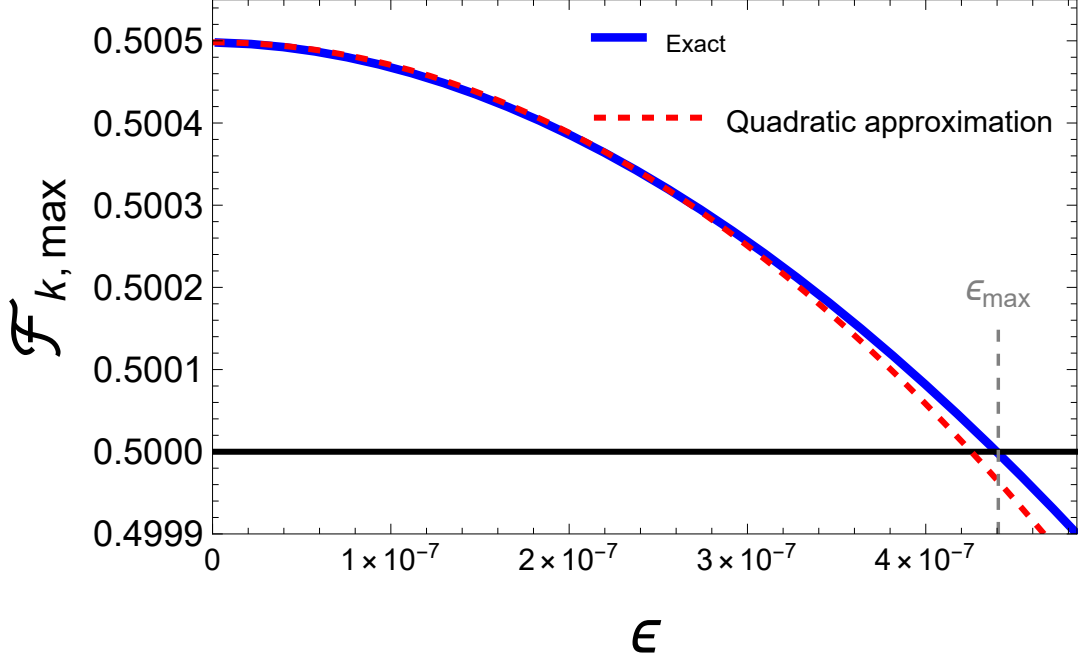


FIG. S.11. Blue continuous line shows the exact numerical evaluation of $\mathcal{F}_{k,\max}$ as a function of ϵ for the exact resonance 1:1, $J = 1000$ and $\tau \approx 8$. Red dashed line is the perturbative approximation up to second order in ϵ , shown in Eq. (S.39). The condition $\mathcal{F}_{a,\max} = 1/2$ (horizontal black line) determines ϵ_{\max} (vertical dashed line).

$\mathcal{F}_{k,\max}$ is very well described by the first term in Eq.(S.56), which indicates that the effect of the term $T_2\epsilon^2$ is rather marginal. Therefore

$$\begin{aligned} \mathcal{F}_{k,\max} \approx (1 - D_o J^4 \epsilon^2) \left(\frac{1}{2} + \frac{\kappa_o}{4\kappa J} \right) &= \left(1 - \epsilon^2 \sum_{k' \neq a, a'} |\langle E_{k'} | f_a^{(1)} \rangle|^2 \right) |\langle E_a | f_a^{(0)} \rangle|^2 \\ &= \left(1 - \frac{\epsilon^2}{4} \sum_{k' \neq a, a'} \frac{|\langle E_{k'} | \hat{K} | f_a^{(0)} \rangle|^2}{\sin^2 \left(\frac{\tau(E_{k'} - E_a)}{2} \right)} \right) |\langle E_a | f_a^{(0)} \rangle|^2, \end{aligned} \quad (\text{S.57})$$

which is the expression shown in main text with $c = \frac{\kappa_o}{4\kappa}$ and $D_o = a_{2,\text{ER}}$.

The scaling of $\epsilon_{k,\max}$ for an exact resonant state can be obtained easily from Eq.(S.57). The maximum perturbation strength is obtained from the condition $\mathcal{F}_{k,\max} = 1/2$, which yields

$$\epsilon_{k,\max} \approx \sqrt{\frac{\kappa_o}{2\kappa J D_o J^4}} = \sqrt{\frac{\kappa_o}{2\kappa D_o}} \frac{1}{J^{5/2}} = C J^{-5/2}. \quad (\text{S.58})$$

This power-law for $\epsilon_{k,\max}$ is confirmed numerically in Fig.3(c) of main text.

We end by noting that, in contrast to non-degenerate unitary perturbation theory, where the perturbative series of $\mathcal{F}_{k,\max}$ up to $\mathcal{O}(\epsilon^2)$ fails to describe the numerical results in the whole range $\epsilon \in [0, \epsilon_{k,\max}]$, degenerate perturbation theory up to $\mathcal{O}(\epsilon^2)$ provides a much more accurate description of $\mathcal{F}_{k,\max}$ in the ϵ -interval of interest. As illustrated in Fig. S.11, the second order approximation to $\mathcal{F}_{k,\max}$ in the degenerate case closely matches the numerical results. This comes from the fact that, in the degenerate case, $\mathcal{F}_{k,\max}$ for infinitesimal ϵ is larger but very close to 1/2.